Geochemistry, Geophysics, Geosystems®

RESEARCH ARTICLE
10.1029/2023GC011074

Special Section:
Through the Arctic Lens: Progress in Understanding the Arctic Ocean, Margins and Landmasses

Shallow Thermal Anomalies and Their Role in the Breakup Evolution Along the Conjugate Margins of the Fram Strait (Svalbard and Eastern North Greenland), Indicated by Low-Temperature Thermochronology

Katrin Meier[1,2], Paul O'Sullivan[3], Malte M. Jochmann[4,5], Tino Wallrath[1], Patrick Monien[1], Karsten Piepjohn[6], Frank Lisker[1], and Cornelia Spiegel[1]

[1]Department of Geosciences, University of Bremen, Bremen, Germany, [2]State Museum of Natural History Karlsruhe (SMNK), Karlsruhe, Germany, [3]GeoSep Services, Moscow, ID, USA, [4]Department of Arctic Geology, University Centre in Svalbard (UNIS), Longyearbyen, Norway, [5]Department of Earth Sciences, University of Bergen, Bergen, Norway, [6]Federal Institute for Geosciences and Natural Resources (BGR), Hannover, Germany

Abstract We investigated highly mature sedimentary rocks exposed along both sides of the Fram Strait in the northern North Atlantic using apatite fission track and (U-Th)/He thermochronology to obtain information on the thermal imprint of rifting and continental breakup processes along a sheared margin. Our data showed that the conjugate margins experienced several heating episodes, which we explain as resulting from heat transfer along segments of the De Geer Fracture Zone, a large continental transform system which connected magmatic centers north and south of the Fram Strait. Heating occurred prior to and during the Eurekan intraplate orogeny, which occupied the position of the present-day Fram Strait during the Eocene. Heat transfer may have caused or contributed to lithospheric weak zones, which focussed deformation during intraplate orogeny. Movements along the transform fault system continued during the Oligocene, after the end of the Eurekan Orogeny, causing further structural weakening of pre-existing fault zones. These were exploited during the final continental breakup leading to the opening of the Fram Strait. No unambiguous thermal signature associated with this latest stage of breakup was detected. Our data underline recent studies on the importance of structural inheritance and continental transform faults for the prolonged and complex processes of continental rifting and breakup.

Key Points:

- Thermal anomalies along the Fram Strait are related to tectonic processes from Late Cretaceous rifting to Miocene continental breakup
- The De Geer Fracture Zone influenced the thermal evolution and structural weakening of the crust, which contributed to the Eurekan orogeny
- Structural inheritance and transform faults influence continental rifting and the development of continental margins

Supporting Information:

Supporting Information may be found in the online version of this article.

Correspondence to:

K. Meier,
k.meier@uni-bremen.de

Citation:

Meier, K., O'Sullivan, P., Jochmann, M. M., Wallrath, T., Monien, P., Piepjohn, K., et al. (2024). Shallow thermal anomalies and their role in the breakup evolution along the conjugate margins of the Fram Strait (Svalbard and eastern North Greenland), indicated by low-temperature thermochronology. *Geochemistry, Geophysics, Geosystems*, *25*, e2023GC011074. https://doi.org/10.1029/2023GC011074

Received 5 JUN 2023
Accepted 23 FEB 2024

1. Introduction

Continental rifting, breakup, and the formation of passive continental margins are complex multistage processes, resulting from the interaction of deformation, and magmatic, thermal and isostatic processes (e.g., Peron-Pinvidic & Manatschal, 2019). They are inevitably associated with heat flow variations, as rifting strongly influences the thermal structure of the lithosphere, and vice versa: Lithospheric extension plus probably associated magmatic activity increases the crustal heat flow, and increased heat flow weakens the crust and thus determines the locus of breakup and facilitates rupture (e.g., Blackwell, 1978; Brott et al., 1981; Chapman & Rybach, 1985; Huismans & Beaumont, 2008; Nemčok, 2016). Understanding the thermal history of passive continental margins is thus important for understanding the processes of rifting, breakup, and margin formation. For this study, we aim to contribute to this understanding by investigating the conjugate margins to both sides of the Fram Strait in the northern North Atlantic, that is, the eastern North Greenland and the western Barents margins (hereafter named "Greenland margin" and "Barents margin"). The Greenland and Barents margins developed along a continental transform fault zone—the De Geer Fracture Zone—which presumably formed already during the Paleozoic (Harland, 1969). It linked two mid-ocean ridges: The Gakkel Ridge of the Arctic Ocean north of the Fram Strait and the Mohns Ridge of the Norwegian-Greenland Sea south of the Fram Strait. Breakup along the De Geer Fracture Zone (DGFZ) resulted in the formation of a sheared margin along the Fram Strait, evolving into a highly oblique divergent margin (Faleide et al., 2008).

The motivation for our study was the observation of strongly enhanced thermal maturities of sedimentary rocks exposed in close vicinity to the coast of either margin (Håkansson et al., 1994; Kleinspehn & Teyssier, 1992; Paech & Estrada, 2019; Paech & Koch, 2001). Along the Greenland margin, Late Cretaceous deposits of the Nakkehoved Formation show vitrinite reflectance (VR) values of up to 7%–10% (Håkansson et al., 1994), corresponding to greenschist-facies temperatures. These maturation values quickly decrease inland (Håkansson

et al., 1994; Håkansson & Pedersen, 2001). Further north along the Greenland margin, Paleocene sedimentary rocks of the Thyra Ø Formation also show increased VR values of >2%, as compared to thermal maturities reported from same-age sedimentary rocks further inland (Håkansson et al., 1994; Paech & Estrada, 2019). A mirror-image situation was observed on the opposite side of the Fram Strait along the Barents margin: On Prins Karls Forland (an island off Spitsbergen forming the northwesternmost subaerial exposure of the Barents Shelf) Paleogene sedimentary rocks show VR values of up to >4% (Kleinspehn & Teyssier, 1992; Paech & Koch, 2001). By contrast, similar-aged deposits exposed on western Spitsbergen only ∼15 km further east across the Forlandsundet Graben display much lower thermal maturities with VR values <1% (Kleinspehn & Teyssier, 1992, 2016; Paech & Koch, 2001).

Håkansson et al. (1994) described the thermal overprint of both the Late Cretaceous and the Paleogene sedimentary rocks exposed along the Greenland margin as being related to the same "thermal event." Based on the youngest stratigraphic age of the affected sedimentary rocks, this proposed event was placed as having occurred during or after the Paleogene (Håkansson et al., 1994; Håkansson & Pedersen, 2001; Paech & Estrada, 2019). The (post-)Paleogene age suggests that the proposed thermal event may have been connected to the Miocene northward propagation of the Knipovich spreading ridge (Dumais et al., 2020; Jokat et al., 2016), initiating the opening of the Fram Strait and the final breakup between North America (Greenland) and Eurasia (Scandinavia). The similar depositional age of the affected sedimentary rocks along the Barents margin and the similar pattern of decreasing maturities away from the coast imply that both conjugate margins may have experienced the same regional-scale thermal history. This also implies that the thermally overprinted sedimentary rocks of both margins recorded the heat flow variations associated with the last stages of continental breakup and incipient sea floor spreading.

For studying the thermal evolution of the conjugate margins, and for bracketing the timing of the proposed thermal event(s), we used apatite fission track (AFT) and (U-Th)/He thermochronology and integrated these data with published VR data by thermal history inversions. Our data will show that, despite the apparent similarities, both margins have experienced a complex and differential thermal history, with several heating episodes all occurring prior to the final continental breakup. We explain our data in terms of heat transfer and movements along the DGFZ, underlining the importance of inherited fault structures and continental transforms for breakup processes (Lundin et al., 2023).

2. Geological Background

2.1. Evolution of the Conjugate Greenland and Barents Margins

The Fram Strait forms the only deep-water connection between the Arctic Ocean and the North Atlantic and is situated along the Greenland and Barents margins (Figure 1). Both margins were formerly continuous and situated within a large dextral continental transform system—the DGFZ. The DGFZ comprises the Senja Fracture Zone, the Vestbakken Volcanic Province and the Hornsund Fault Zone (from south to north along the Barents margin; e.g., Faleide et al., 2008; Gabrielsen et al., 1990; Ryseth et al., 2003), the Greenland Fracture Zone (separating the Boreas and the Greenland Basin within the Norwegian-Greenland Sea; e.g., Døssing et al., 2008; Faleide et al., 1993; Mosar et al., 2002); the Trolle Land Fault Zone (in eastern North Greenland; e.g., von Gosen & Piepjohn, 2003; Håkansson & Pedersen, 2001; Svennevig et al., 2016), and has presumably continued further west, across northern Ellesmere Island (Piepjohn et al., 2016; Vamvaka et al., 2019) and along the northern margin of the Canadian Arctic archipelago (Lundin et al., 2023). Movements along a precursor of the DGFZ presumable commenced already during the Paleozoic (Dallmann, 2015; Harland, 1969). The DGFZ became active as a dextral transform fault in the Late Cretaceous, accommodating the onset of rifting in the Eurasian Basin and in the future Norwegian-Greenland Sea (Srivastava, 1978). Continental rifting preceding the opening of the Eurasia Basin was associated with trachytic to rhyolitic volcanism in North Greenland during the latest Cretaceous (Kap Washington Group volcanic sequence Estrada et al., 2001; Tegner et al., 2011; Thórarinsson et al., 2011).

During the Paleocene, seafloor spreading commenced in the Baffin Bay/Labrador Sea area west of Greenland (Oakey & Chalmers, 2012). In the early Eocene, spreading also initiated along the Aegir and Mohns Ridges of the Norwegian-Greenland Sea (Gernigon et al., 2012), and along the Gakkel Ridge of the Eurasia Basin (Arctic Ocean, Schreider et al., 2019; Vogt et al., 1979). Extensional movements associated with seafloor spreading in the Arctic and in the Norwegian-Greenland Sea were accommodated by the right-lateral continental DGFZ, which

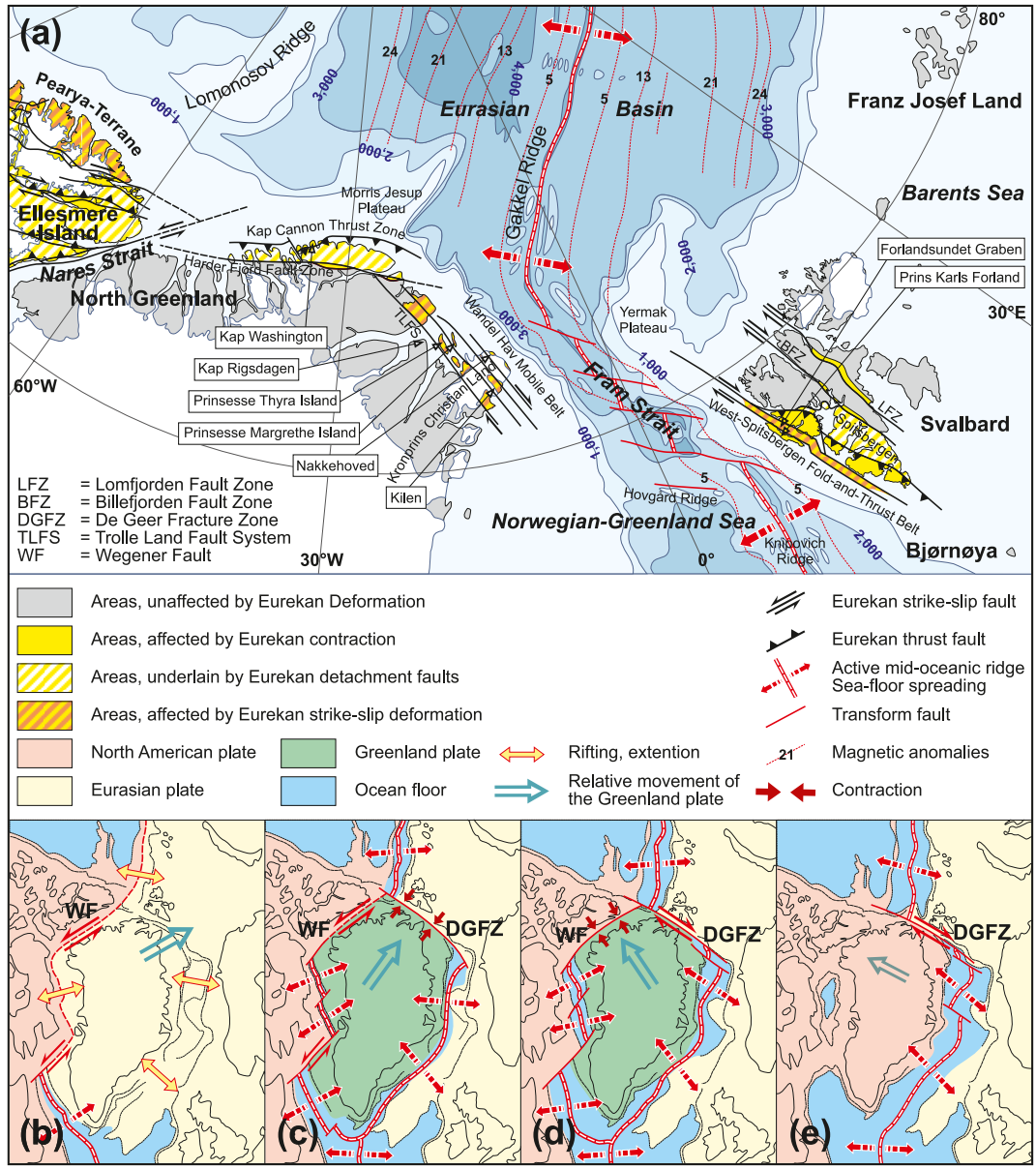

Figure 1. Map showing the areas affected by the Eurekan deformation and the associated structures (a) and the two phase model after Piepjohn et al. (2016) illustrating the plate configuration causing the Eurekan structures with (b) the pre-Eurekan stage; (c) first stage of Eurekan deformation with NE-SW contraction along the present west coast of Spitsbergen and contemporaneously sinistral strike-slip movements along the NE-SW striking Wegener Fault (WF) between Northwest Greenland and Ellesmere Island; (d) second stage of Eurekan deformation with NW-SE dextral strike-slip motions along the De Geer Fracture Zone (DGFZ) between Northeast Greenland and Svalbard and NW-SE contraction across Nares Strait on Ellesmere Island; (e) post-Eurekan stage with further motion along the DGFZ.

connected both spreading ridges. As a result of contemporaneous spreading east and west of Greenland, Greenland moved north, converging with West Svalbard and Ellesmere Island (Figures 1c and 1d). This caused the formation of the intraplate Eureka Orogen during the Eocene. Deformation was focused along the DGFZ and an associated continental transform fault zone, the Wegener Fault along the Nares Strait (Figures 1c and 1d), resulting, amongst others, in the formation of the West Spitsbergen Fold-and-Thrust Belt and the Wandel Hav Mobile Belt (Figure 1a; Piepjohn et al., 2016).

Driven by changes in spreading rates and directions in the Norwegian-Greenland Sea and associated movements of Greenland, Eurekan deformation comprised several stages. The first Eurekan stage was dominated by NE-SW

compression along the DGFZ (Figure 1c), changing to transpression during the second Eurekan stage (Figure 1d). Based on thermochronological studies in Pearya, the two stages of Eurekan Orogeny were accompanied by episodic exhumation between 55-48 Ma and 44-38 Ma (Vamvaka et al., 2019). Due to the high degree of obliquity, the style of deformation differed along the DGFZ. Compression and transpression along the northern segments of the DGFZ, associated with the formation of the West Spitsbergen Fold-and-Thrust Belt, was coeval with transtension along the southern segments of the DGFZ (central to southern Barents shelf), leading to dextral pull-apart basin formation and associated intense magmatic activity of the Vestbakken Volcanic Province (Libak et al., 2012; Lundin et al., 2023).

When spreading in the Labrador Sea/Baffin Bay west of Greenland ceased at c. 33 Ma (Engen et al., 2008; Faleide et al., 2008; Talwani & Eldholm, 1977), the resulting new stress regime caused a change to predominantly transtensive movements along the DGFZ (Figure 1e). These movements were again associated with enhanced exhumation (post-Eurekan stage, ∼34-26 Ma; Vamvaka et al., 2019). Presumably during the early Miocene, the Knipovich Ridge formed (Dumais et al., 2020; Jokat et al., 2016) and propagated toward the north into the area of DGFZ, initiating the final continental break up and dissection of the Eurekan Belt. This led eventually to the opening of the Fram Strait, connecting the spreading centers of the Arctic and the North Atlantic oceans. During the middle Miocene, the Greenland and Barents margins experienced uplift (Bonow & Japsen, 2021; Dörr et al., 2013; Dörr, Lisker, Piepjohn, & Spiegel, 2019; Japsen et al., 2023), associated with a regional unconformity in the offshore seismic record (Døssing et al., 2016), and accompanied by magmatic activity (Geissler et al., 2019; Prestvik, 1978; Sushchevskaya et al., 2009). Døssing et al. (2016) related these changes to a changed stress regime along the Greenland Fracture Zone-segment of the DGFZ, coeval with accelerated widening of the Fram Strait.

2.2. Sedimentary Rocks of the Wandel Sea Basin, Greenland Margin

Sedimentary successions of the Wandel Sea Basin in eastern North Greenland unconformably overlie folded and metamorphosed rock units of the Neoproterozoic to Silurian Franklinian Basin (Dawes & Soper, 1973; Higgins et al., 1981; Soper & Higgins, 1987, 1991; Thorsteinsson & Tozer, 1970). Their tectonic evolution was mostly controlled by dextral kinematics along the Trolle Land Fault System (Håkansson & Schack Pedersen, 1982). Håkansson and Schack Pedersen (1982, 2015) interpreted the local sedimentary occurrences within the Wandel Sea Basin as different syn-tectonic pull-apart basins formed by several dextral strike-slip events with late Cretaceous deformation. According to von Gosen and Piepjohn (2003), strike-slip deformation is mostly concentrated along the faults of the Trolle Land Fault System, presumably related to the Eurekan deformation. Svennevig et al. (2016) supported this suggestion but emphasized a compressional component associated with the deformation.

Sedimentation in the Wandel Sea Basin started in the early Carboniferous with the deposition of sandstones, partly red conglomerates and evaporitic rocks, followed by thick late Carboniferous to Permian limestones and cherts, Triassic and Jurassic dark shales and siltstones, and the Early Cretaceous sandstones and siltstones of the Ladegårdsåen Formation (Bjerager et al., 2019; Håkansson et al., 1991; Hovikoski et al., 2018). During the latest Cretaceous, the Kap Washington Group was deposited in North Greenland, containing volcanic and pyroclastic rocks associated with rift-related magmatism (Estrada et al., 2001; Tegner et al., 2011; Thórarinsson et al., 2011). The Kap Washington Group has the same stratigraphic age as the Nakkehoved Formation further south, exposed along the north-eastern coast of Kronprins Christian Land (Figure 2a). The Nakkehoved Formation is composed of monotonous, dark gray, fine-grained marine sandstones to greywackes, in places very rich in feldspar. It contains a sparse bivalve fauna, on which the late Cretaceous age of the formation is based (Håkansson et al., 1981). Svennevig et al. (2018) assign a Maastrichtian age to the Nakkehoved Formation in their revised stratigraphy of Kronprins Christian Land. The Nakkehoved Formation differs from neighboring successions of the same stratigraphic age exposed in the Kilen area (Figure 2a) in terms of the high amount of feldspar and due to the "totally distinct" fauna (Håkansson & Schack Pedersen, 2015).

The Nakkehoved Formation also differs from all other deposits of the Wandel Sea Basin regarding its thermal maturation, which indicates post-depositional heating to temperatures of 200–300°C. This estimate is based on VR values between 7% and 10%, newly grown albite and chlorite, illite crystallinity, and the complete degradation of organic-walled microfossils (Håkansson et al., 1994). Apparently restricted to a single nunatak, a "dense swarm of quartz veins" occurs in the Nakkehoved Formation (Håkansson et al., 1994). Its formation is interpreted as being associated with the post-depositional thermal overprint of the Nakkehoved Formation (Håkansson

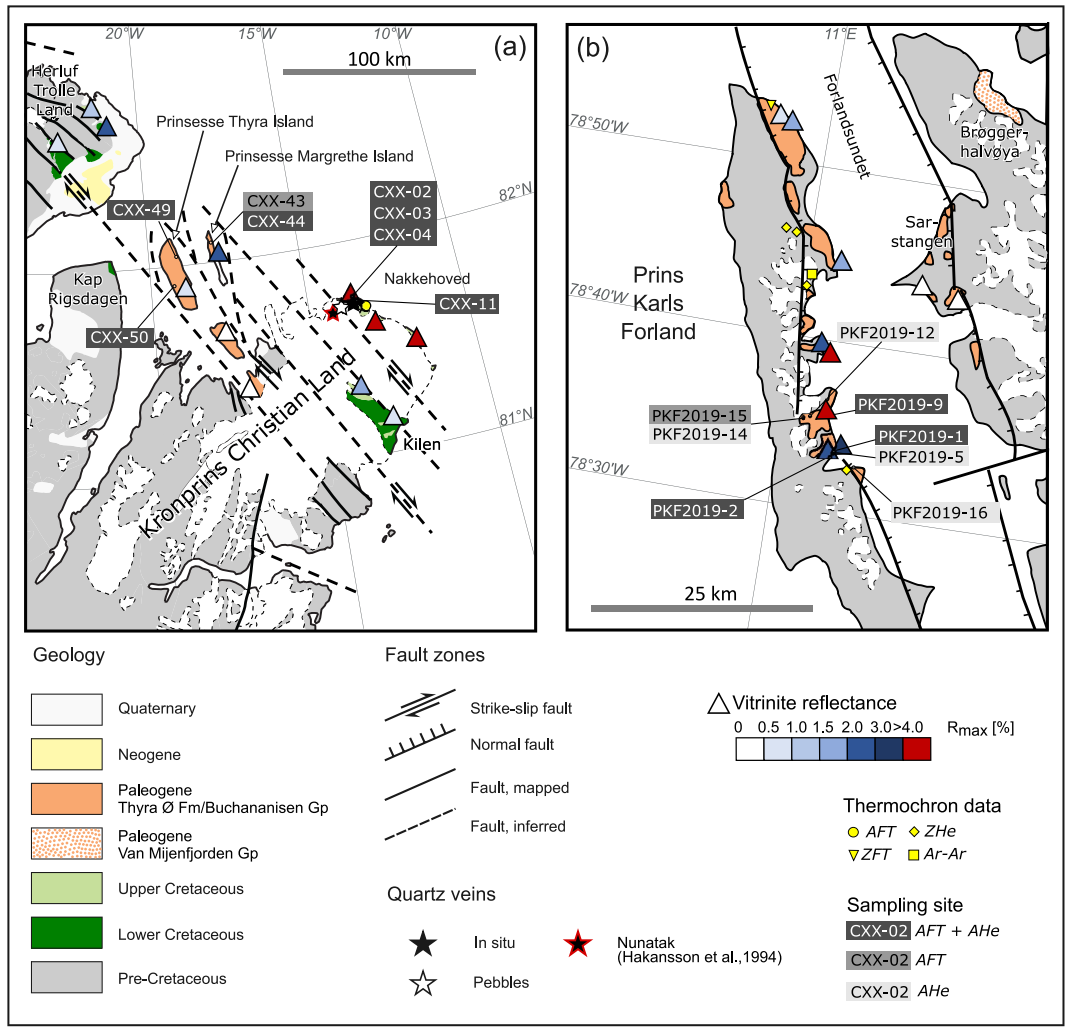

Figure 2. Geological maps of the study areas on the conjugate margins of eastern North Greenland (a) and western Svalbard (b) with thermal maturities published by Håkansson et al. (1994), Kleinspehn and Teyssier (1992), Paech and Estrada (2019), and Paech and Koch (2001) decreasing to the hinterland (maps redrawn and compiled after Dallmann, 2020, Japsen et al., 2021; Piepjohn et al., 2016). Sample locations are marked as well as locations of published thermochronological data by Schneider et al. (2019) (square), Blythe and Kleinspehn (1998) (triangle, circle), Barnes and Schneider (2019) (diamond) and Japsen et al. (2021) (circle). The location of the outcrop with quartz vein occurrence is marked with the black star next to the sample locations of CXX-02, CXX-03, CXX-04 and CXX-11 (Figure S1 in Supporting Information S1).

et al., 1994). Fluid inclusions in quartz indicate a crystallization depth of the veins of only 200–300 m (Håkansson et al., 1994). These shallow crystallization depths, along with the very modest deformation of the rocks and the lack of any metamorphic fabric, suggest a purely thermal origin of the high post-depositional temperatures (Håkansson et al., 1994).

Northwest of Nakkehoved, Paleogene sedimentary rocks of the Thyra Ø Formation are exposed (Figure 2a), mostly along three small islands named Prinsesse Margrethe Island, Prinsesse Thyra Island and Prinsesse Dagmar Island (Prinsesse Islands in the following). The basis of the Thyra Ø Formation beneath the Prinsesse Islands is unknown, but further west at Kap Rigsdagen (Figure 2a), the Thyra Ø Formation unconformably overlies Early Cretaceous deposits of Barremian age (Piasecki et al., 2018).

The Thyra Ø Formation consists of alternating sandstones and shales with intercalated thin coal seams and possibly altered volcanic ash layers (Paech & Estrada, 2019). The fluvial to marine, undeformed, greyish sedimentary rocks are bedded horizontally to slightly inclined. For Prinsesse Margrethe Island, Håkansson et al. (1981) described a coarse, block-supported conglomerate with interbedded sandstone channel fills in a single

isolated outcrop. Particularly the southeasternmost exposures of the Thyra Ø Formation contain fossil plant material (e.g., Boyd, 1990) and dinoflagellate cysts, which show increasing corrosion toward the northeast. Hence, the deposits of Prinsesse Margrethe Island are void of palynomorphs (Lyck & Stemmerik, 2000). Based on its fossil content, the Thyra Ø Formation was dated as late Paleocene to earliest Eocene on the Prinsesse Islands (Lyck & Stemmerik, 2000), and as early to middle Eocene at Kap Rigsdagen (Piasecki et al., 2018).

For Prinsesse Margrethe Island, Håkansson et al. (1994) reported a VR value with Rmax of about 2%. This analysis is based on nine measurements only and therefore needs to be viewed with caution. VR values of the Thyra Ø Formation at other localities range between 0.4% and 0.65% (Figure 2a) and were interpreted as being related to burial (Håkansson et al., 1994; Paech & Estrada, 2019). The higher maturation value of Prinsesse Margrethe Island, by contrast, was explained as related to the same post-depositional "thermal event" that also caused the high maturation of the Nakkehoved Formation and which may have extended to Kilen further south (Figure 2a; Håkansson et al., 1994). Igneous activity as a heat source for this proposed thermal event was considered as unlikely, because magmatic bodies are not known in Kronprins Christian Land and because—according to these authors—accessory minerals were completely lacking in the quartz veins of Nakkehoved. Instead, they suggest increased heat flow due to crustal thinning or the initiation of spreading at the Knipovich ridge. Paech and Estrada (2019) restricted the extent of the thermal overprint to Nakkehoved and Prinsesse Margrethe Island and also attributed the increased heat flow to the active plate boundary between northeast Greenland and Svalbard. Japsen et al. (2021) suggest localized warming or differential exhumation as a cause and a Late Cretaceous or Paleocene age based on AFT data of a sample from Nakkehoved. Pedersen et al. (2018), who studied thermal overprinting in Kilen, concluded that the maximum temperature there must have been reached after the Santon and before the Eurekan deformation, however, as a result of sedimentary burial.

2.3. Sedimentary Rocks of the Forlandsundet Area, West Svalbard, Barents Margin

In Svalbard, a (post-) Carboniferous sedimentary sequence overlies folded and thrust-faulted Devonian redbeds and pre-Devonian sedimentary and metamorphosed basement rocks (Dallmann, 2015; Frebold, 1935; Harland, 1997; Orvin, 1940). Between the Carboniferous and the Early Cretaceous, the basins of Svalbard and eastern North Greenland evolved in a similar way, but from the Late Cretaceous onwards, both areas experienced different geological developments: While Late Cretaceous deposits are widely exposed in North Greenland (e.g., in Nakkehoved, Kilen, or in the Kap Washington area), they are lacking on Svalbard (except for a possible occurrence in the Sørkapp Land of Spitsbergen; Krutzsch, 2001; Smelror & Larssen, 2016). During the Late Cretaceous, North Svalbard and the wider area of the Barents Shelf experienced a period of enhanced exhumation (Dörr et al., 2012; Dörr, Lisker, Piepjohn, & Spiegel, 2019; Japsen et al., 2023; Lasabuda et al., 2021). Paleogene deposition started with the Paleocene to Eocene coastal to shallow marine sandstones, siltstones and shales of the Van Mijenfjorden Group and its equivalents in the Central Tertiary Basin and on Brøggerhalvøya, respectively (Figures 2b and 3; Dallmann, 1999, 2015).

In the Forlandsundet area, that is, on Prins Karls Forland and on Spitsbergen along the western coast of the Forlandsundet Graben (Figure 2b), the sedimentary sequences of the Buchananisen Group are exposed. The Buchananisen Group comprises a clastic sedimentary succession, which lies unconformably on top of a pre-Devonian basement (Dallmann, 1999, 2020; Kleinspehn & Teyssier, 1992). According to Dallmann (1999 and references therein), the colorful conglomerates with up to boulder-sized angular clasts of the Selvågen Formation form the basis conglomerate on Prins Karls Forland and are interpreted as alluvial fanglomerates. They are overlain by the Sesshøgda, Reinhardpynten, Krokodillen, Marchaiselaguna and the Aberdeenflya Formations, which are built up by coarse to fine sandstones alternating with clay and siltstones and conglomeratic layers and represent alluvial to shallow marine deposits (Figure 3). The exposures east of the graben comprise the Sarsbukta and Sarstangen conglomerates. The Sarstangen conglomerates are less consolidated compared to the other deposits, lack deformation and are the only formation directly palynologically dated to be of Oligocene age (Kleinspehn & Teyssier, 2016; Schaaf et al., 2021; Figure 3).

Generally, the stratigraphic ages of the Buchananisen Group and of its individual formations are poorly defined. Due to thermal overprinting, microfossils are lacking or poorly preserved (e.g., Čepek, 2001; Manum & Throndsen, 1986). Deposition in the Forlandsundet Basin started prior to the formation of the Forlandsundet Graben in the late Eocene/early Oligocene (Blinova et al., 2009; Kleinspehn & Teyssier, 1992). Based on stratigraphic relationships and the general tectonic development recorded by the Cenozoic deposits on Svalbard,

10.1029/2023GC011074

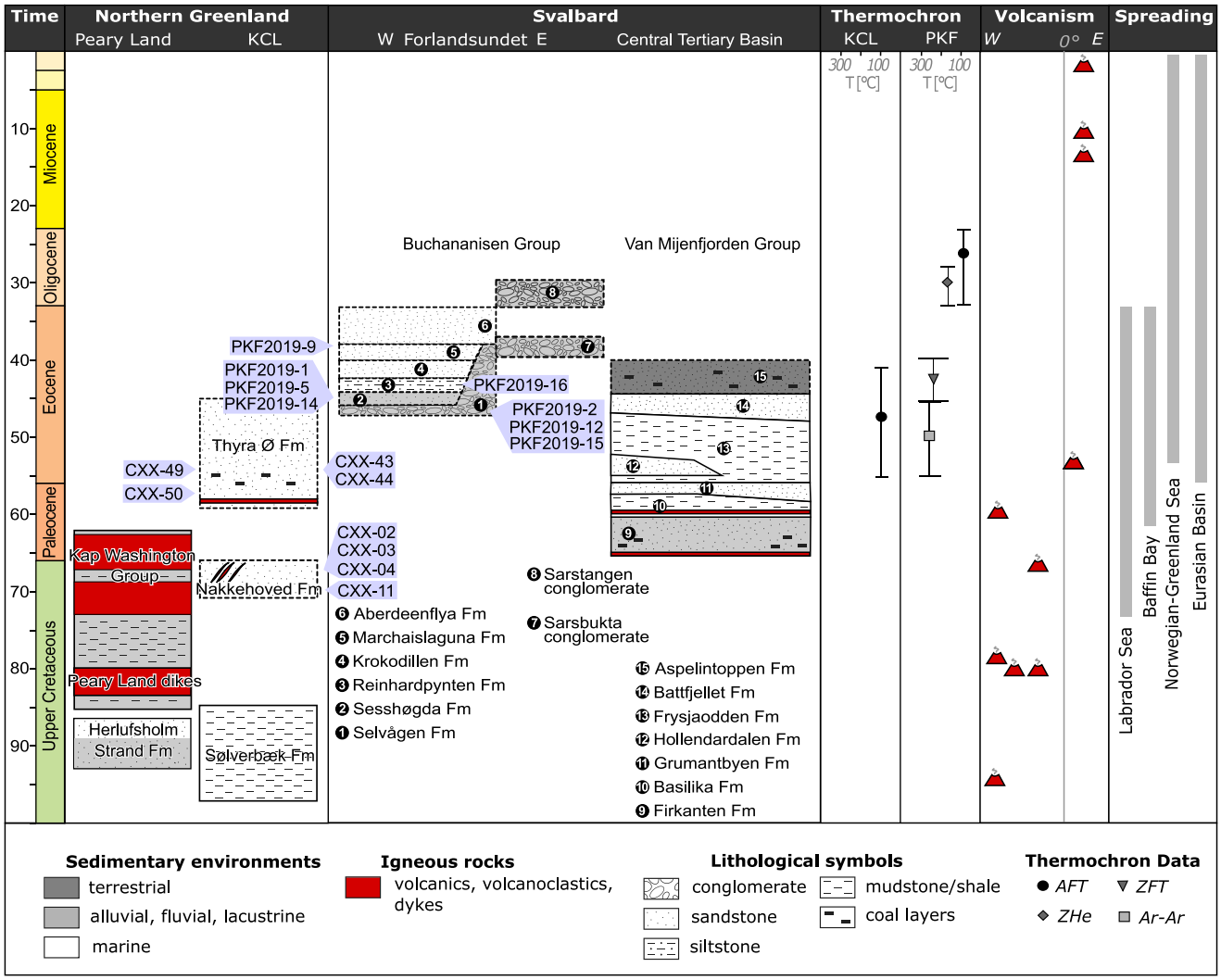

Figure 3. Overview of the Late Mesozoic and Cenozoic stratigraphy of North Greenland and Svalbard, published thermochronological data, temporal and spatial occurrence of volcanism in the High Arctic and spreading activity. Stratigraphy is based on Dallmann (1999, 2015, 2020), Dörr, Lisker, Jochmann, et al. (2019), Håkansson et al. (1981), Kleinspehn and Teyssier (2016), Lyck and Stemmerik (2000), Piasecki et al. (2018), Schaaf et al. (2021), Svennevig et al. (2018), and Thórarinsson et al. (2015) with dotted lines showing uncertain depositional ages. Volcanic deposits and dated/correlated ash layers are marked in red (ash layers in Van Mijenfjorden Group dated by Jones et al. (2016), ash layer in Thyra Ø Fm correlated by Paech and Estrada (2019)). Thermochronological data include range of Ar-Ar ages by Schneider et al. (2019) (square), a zircon fission track age by Blythe and Kleinspehn (1998) (triangle), zircon (U-Th)/He ages by Barnes and Schneider (2019) (diamond) and Apatite fission track ages by Blythe and Kleinspehn (1998) and Japsen et al. (2021) (circle). The time and location of volcanism are based on Døssing et al. (2013), Estrada et al. (2010), Riefstahl et al. (2013) and Senger et al. (2014) and the spreading activity is based on Gernigon et al. (2012). KCL, Kronsprins Christian Land.

the possible age of the deposits ranges from late Paleocene to early Oligocene (Dallmann, 1999, 2015; Gabrielsen et al., 1992; Kleinspehn & Teyssier, 1992; Livšic, 1974, 1977, 1992). According to Dallmann (2020), the basement of Prins Karls Forland was deformed by the first stage of Eurekan compression. The deformation of the overlying sediments of the Buchananisen Group, however, was associated with the second stage of the Eurekan (cf. Piepjohn et al., 2016). These observations suggest that the Buchananisen Group on Prins Karls Forland was deposited during/after the first stage of the Eurekan orogeny (i.e., (post) early Eocene) but pre-Oligocene (i.e., prior to the end of second stage of the Eurekan). Hence, an Eocene (~56–33 Ma) depositional age is most likely for the Buchananisen Group on Prins Karls Forland.

The thermal overprint of the Buchananisen Group is restricted to the exposures of Prins Karls Forland, west of the Forlandsundet Graben (Figure 2b). Here, VR values between 2% and 5% were reported (Kleinspehn & Teyssier, 1992; Paech & Koch, 2001), corresponding to paleotemperatures of more than 200°C. By contrast, exposures

of the Buchananisen Group east of the Forlandsundet Graben show VR values <1% (Figure 2b). At the sites of the highest VR values, Kleinspehn and Teyssier (1992) also describe localized ductile fabrics such as foliation and deformation bands. They interpreted the high maturation in terms of a deeper burial west of the Forlandsundet Graben as compared to the eastern side. This is in agreement with zircon (U-Th)/He ages from the basement of Prins Karls Forland and from the West Spitsbergen Fold-and-Thrust Belt, which suggest that the West Spitsbergen Fold-and-Thrust Belt cooled from the middle Eocene onwards, whereas Prins Karls Forland remained at higher temperatures and may thus represent a deeper structural level of the fold belt (Barnes & Schneider, 2019). Paech and Koch (2001) suggested that the high maturation was influenced by tectonic deformation and convective heat supply, likely due to a nearby spreading center.

3. Material and Methods

3.1. Sampling Strategy, Field Observations and Description of the Sampled Material

Sampling in North Greenland was carried out in 2018, during expeditions CASE 20 and RV Polarstern cruise PS115/1, organized by the Federal Institute for Geosciences and Natural Resources. The samples from Prins Karls Forland were collected in 2019 during a cruise with RV Clione. We aimed to take samples from Late Cretaceous and Paleogene strata for which high VR values were previously reported by Håkansson et al. (1994) and Paech and Koch (2001) (Figures 2a and 2b). In North Greenland, we sampled two sites on Prinsesse Thyra Island, one site on Prinsesse Margrethe Island, and several locations at Nakkehoved, including specimens of the quartz veins (Figures 2a, Table S1 in Supporting Information S1). Unlike previous descriptions in the literature (e.g., Håkansson et al., 1994; Japsen et al., 2021), we found that quartz veins within the Nakkehoved Formation are not restricted to a single exposure but also occur in situ in another outcrop of the Nakkehoved Formation in Kronprins Christian Land (Figures 2a, Table S1 and Figure S1 in Supporting Information S1).

On Prinsesse Thyra Island, the sampled strata differed between the eastern and the western coast: In the west, the sandstones were weakly lithified (CXX-50), whereas in the east, the sandstones were stronger lithified (CXX-49). On Prinsesse Margrethe Island, we took samples of mid-to coarse-grained sandstones of the Thyra Ø Formation from a site close to a small stream (CXX-43, CXX-44). Because of the extensive snow cover, we could not sample in situ exposures, but due to the abundance of only a single rock-type, due to the angular platy appearance of the rocks, and because of the relatively weak lithification of the Thyra Ø formation elsewhere in the Wandel Sea basin, which would prevent transport of larger rock slabs, we are confident that the material originated from Prinsesse Margrethe Island. On Prins Karls Forland, we sampled two transects across the Buchananisen Group, focusing on areas for which high maturation values were published (Paech & Koch, 2001). One sample from the Marchaiselaguna Formation (PKF2019-9) was taken from an outcrop showing intense deformation accompanied by carbonate veins.

The samples (including host rocks along with quartz veins from Nakkehoved) were investigated for indications of thermal exposure by thin section microscopy and supporting electron microprobe analysis. The host rocks of the quartz veins show signs of quartz mobilization, feldspar sericitization and growth of chlorite and epidote. All these corroborate a thermal overprint of the host rock with temperatures between at least 200°C and 300°C. In contrast to previous descriptions, the quartz veins are not composed purely of quartz but contain minor amounts of feldspar, carbonate, chlorite, biotite and muscovite, hematite, rutile and ilmenite. This may indicate the involvement of (magmatism-related?) fluids during post-depositional heating. The samples from Prinsesse Margrethe Island also show sericitization and chloritization. By contrast, only weak indications for thermal exposure were found in samples from Prinsesse Thyra Island. Details are reported in the Supporting Information S1.

3.2. Methods

Apatite fission track and apatite (U-Th)/He (AHe) analyses are thermochronological methods, that is, they are temperature-sensitive radiometric dating methods. AFT analysis is based on the spontaneous fissioning of uranium, resulting in lattice damages (=fission tracks), which accumulate with time. AHe thermochronology is based on the accumulation of He in the crystal lattice, resulting from the alpha decay of U, Th and Sm. The temperature sensitivity of both thermochronometers is in the low temperature range, that is ~120–60°C for AFT (Wagner et al., 1989) and ~85–40°C for AHe (Wolf et al., 1998). From AFT and AHe data, time-temperature paths are derived by thermal history inversions (e.g., Ketcham, 2005). Cooling and heating can be either

interpreted as exhumation or burial due to tectonic processes or may reflect changes in the geothermal heat flow, for example, due to magmatic activity or crustal thinning.

AFT analysis was carried out by GeoSep Services using standard procedures for the laser-ablation inductively coupled plasma mass spectrometer (LA-ICP-MS) method (Donelick et al., 2005; Hasebe et al., 2004). Apatites were mounted and etched with 5.5 M HNO_3 for 20 s. For track length analysis ^{252}Cf irradiation was used. For kinetic information, Dpar values were measured. Only single-grain AFT ages with U-concentration >0.1 ppm were considered for central age determination with IsoplotR (Vermeesch, 2018). Single-grain AHe analysis was performed in the laboratory facilities of Bremen University. Raw AHe ages were corrected for alpha-ejection (Farley et al., 1996) using the stopping distance of Ketcham et al. (2011). Details on the analytical procedures are described in the Supporting Information S1. Apatite can be affected by radiation damage, which influences He diffusion and retention and causes a trend of older AHe ages with increasing effective Uranium (eU) content (Shuster et al., 2006). In apatite crystals with low eU, He implantation by U-rich neighboring minerals can also lead to the inverse trend, that is, AHe ages become older with decreasing eU content (Spiegel et al., 2009). The AHe ages were checked for these relationships (Figure S4 in Supporting Information S1).

For thermal history modeling, we used the HeFTy software package (Ketcham, 2005) with the annealing model of Ketcham et al. (2007b) applying c-axis projection. Although no positive relationship between eU and AHe age was observed, the influence of radiation damage cannot be ruled out and we applied the diffusion model of Flowers et al. (2009) in general, but in some cases also the diffusion model of Farley (2000). The software's algorithm generates time-temperature paths and predicts the corresponding AFT and AHe data using a Monte Carlo approach. The predicted data are compared to the data observed and classified using the 'goodness-of-fit' (GOF) value. We aimed for models representing the geological and the general thermal history of the investigated area incorporating independent information as constraints, such as VR data and depositional ages (Figures 2 and 3). In case of unclear depositional ages, we used the broadest time frame compiled from the literature and–in case of Nakkehoved–tested, both depositional ages reported in the literature, that is, the more loosely defined Late Cretaceous depositional age suggested by Håkansson et al. (1981), and the Maastrichtian depositional age suggested by Svennevig et al. (2018). Also for Nakkehoved, three of the four samples that contained apatite suitable for AFT and AHe thermochronology were derived from slightly different lithologies of the same outcrop. As all three samples are expected to provide the same thermal history, the Nakkehoved models are particularly well constrained. We allowed heating to temperatures as high as indicated by VR values using the conversion of Burnham and Sweeney (1989) and tested whether the data allowed late Miocene cooling. Input parameters used for thermal history inversions are summarized in Table S3 in Supporting Information S1.

4. Results and Interpretations

4.1. AFT and AHe Results

AFT ages and mean track lengths (MTL) were obtained from eight samples from North Greenland and four samples from Prins Karls Forland. The results are shown in Table 1. AFT central ages range between 23 ± 5 Ma and 67 ± 9 Ma and MTL range between 12.8 and 13.7 μm (reported here without c-axis projection; note that for thermal history inversions, MTL with c-axis projections were used). AHe ages were obtained from 14 samples (seven from both North Greenland and Prins Karls Forland), providing 34 single grain AHe ages, which range between 21 ± 1 Ma and 106 ± 5 Ma. The results are shown in Table 2.

The distributions of AFT and AHe ages of Nakkehoved, the Prinsesse Islands, and Prins Karls Forland differ, indicating differential thermal histories. Nakkehoved yielded the oldest ages with AFT ages between 58 and 67 Ma and well-replicated AHe ages between 43 and 57 Ma. Slightly younger AFT ages were obtained from the Thyra Ø formation, with a trend of older ages toward the west, although the AFT ages overlap within uncertainty limits: The samples from Prinsesse Margrethe Island yielded AFT ages of 52 and 61 Ma. The sample from the more lithified exposure from the eastern side of Prinsesse Thyra Island also yielded an AFT central age of 61 Ma, whereas the sample from western Prinsesse Thyra Island yielded an AFT age of 69 Ma. This is older than the depositional age of the Thyra Ø Formation and suggests that the AFT system was only partially reset post-deposition, in agreement with the VR values reported from western Thyra Island (Håkansson et al., 1994; Paech & Estrada, 2019). Furthermore, this sample seems to contain two different age populations (see Figure S2 in Supporting Information S1). In contrast, the AHe ages of eastern Prinsesse Thyra Island (37–40 Ma) and from Prinsesse Margrethe Island (29–40 Ma) are older than those of western Prinsesse

Table 1
Results of AFT Analysis

Sample	n[a]	ΣNs[b]	ΣΩ[c] [μm²]	ΣP[d]	U (±SD) [ppm]	Pooled age ±1σ [Ma]	Central age ±1σ [Ma]	P(χ)²	MSWD	MTL [μm] (n)[e]	av. Dpar [μm]
	Nakkehoved, 81° 44.257′N 13° 30.028′ W 137 m, Nakkehoved Fm: greywacke, Upper Cretaceous/Maastricht										
CXX-02	22	291	60,427	1.25	17.4 (±22.3)	62 ± 8	58 ± 10	0	4.1	13.3 ± 1.4 (34)	1.9
CXX-03	40	640	84,694	3.95	28.2 (±44.9)	59 ± 6	67 ± 9	<0.1	1.9	13.7 ± 1.5 (85)	1.9
CXX-04	40	701	105,225	3.57	31.0 (±70.4)	62 ± 5	65 ± 8	0	2.1	13.6 ± 1.6 (68)	1.9
CXX-11	Nakkehoved, 81° 43.381′ N 13° 22.676″ W 432 m, Nakkehoved Fm: greywacke, Upper Cretaceous/Maastricht										
	40	661	106,438	3.54	20.2 (±38.1)	62 ± 6	66 ± 18	0	13	13.6 ± 1.6(102)	1.8
	Prinsesse Margrethe Island, 82° 04.609′ N 17° 47.223′ W 47 m, Thyra Ø Fm: sandstone, Paleocene-Eocene										
CXX-43	28	434	60,524	3.71	32.4 (±26.5)	44 ± 5	52 ± 9	0	2.7	13.3 ± 1.4 (47)	1.9
CXX-44	40	318	93,236	2.64	47.0 (±222.0)	49 ± 7	61 ± 11	<0.1	1.6	13.1 ± 1.7 (60)	2
CXX-49	Prinsesse Thyra Island, 82° 02.074′ N 19° 02.747′ W 12 m, Thyra Ø Fm: sandstone, Paleocene-Eocene										
	39	674	90,324	4.75	23.9 (±24.7)	57 ± 5	61 ± 6	<0.1	1.6	12.8 ± 1.5(70)	2.1
	Prinsesse Thyra Island, 81° 52.359′ N 19° 07.717′ W 25 m, Thyra Ø Fm: sandstone, Paleocene-Eocene										
	40	196	123,328	1.08	71.7 (±460.4)	59 ± 7	69 ± 12	0.85	0.8	13.1 ± 1.6 (87)	2.2
PKF2019-1	Reinhardpynten, 78° 33.4560′ N 11° 16.9040′ E 17 m, Sesshøgda Fm: coarse sandstone, Eocene										
	24	240	65,183	3.45	57.6 (±134.4)	24 ± 4	28 ± 5	<0.1	1.9	13.0 ± 1.6 (49)	1.9
PKF2019-5	Reinhardpynten, 78° 33.4140′ N 11° 16.6030′ E 14 m, Sesshøgda Fm: coarse sandstone, Eocene										
	21	165	37,178	3.13	77.7 (±98.8)	27 ± 5	28 ± 10	0	4.5	13.6 ± 1.6 (30)	2
PKF2019-9	Peter Winterbukta, 78° 35.5770′ N 11° 13.2710′ E 2 m, Marchaiselaguna Fm: fine sandstone, Eocene-Oligocene										
	39	354	103720	4.36	36.8 (±64.4)	26 ± 3	27 ± 6	0	4.1	13.3 ± 2.2 (109)	2
PKF2019-15	Krokodillen, 78° 35.1110′ N 11° 6.7250′ E 235 m, Selvågen Fm: conglomerate, Eocene										
	23	320	58,534	4.45	61.3 (±51.4)	23 ± 3	23 ± 5	0	2.3	13.3 ± 2.3 (44)	2

[a]n = Number of counted grains with U composition >0.1 ppm. [b]ΣNs = Sum of counted spontaneous tracks in analyzed grains. [c]ΣΩ [μm²] = Sum of area with counted tracks in analyzed grains, for comparison: laser spot size 20 μm–ablated area ~314 μm². [d]ΣP = Sum of individual 238U/43Ca ratios of analyzed grain areas. [e]MTL [μm] (n) = Mean track length ± standard deviation (number of measured tracks).

Thyra Island (~27 Ma, excluding the 103 and 106 Ma AHe ages, which are regarded as outliers; Table 2). Compared to the thermochronological ages of the Prinsesse Islands, AFT and AHe ages from Prins Karls Forland are younger (Tables 1 and 2): AFT ages range between 23 and 28 Ma, whereas AHe ages from Prins Karls Forland range between 20 Ma and 51 Ma and show over-dispersion. A negative correlation of AHe ages with the eU content indicates an influence of extraneous He on the AHe ages (Spiegel et al., 2009). The use of broken grains contributed to the dispersion (Beucher et al., 2013; Brown et al., 2013), which is visible in the eU-He plot (Figure S4 in Supporting Information S1). We assume that the youngest AHe ages with the highest eU contents are least influenced by extraneous He; nevertheless, an effect of He implantation cannot be ruled out. Therefore, AHe ages from Prins Karls Forland were not included as input data for thermal history modeling.

Interpretation of the thermal maturity data suggests that the sedimentary rocks exposed in Nakkehoved, on Prinsesse Margrethe Island and on Prins Karls Forland have experienced post-depositional temperatures sufficient to fully reset the AFT and AHe systems. Hence, heating to maximum temperatures must have occurred in the time period between deposition and the AFT date of the sample (Figure 4 left). For Nakkehoved, the Prinsesse Islands and Prins Karls Forland, AFT ages are close to the depositional ages, and even without thermal history inversions, two conclusions can be drawn from the data: (a) The Nakkehoved area experienced heating prior to the Prinsesse Islands, which in turn may have experienced heating prior to Prins Karls Forland, in disagreement to previous assumptions of contemporaneous heating. (b) Heating occurred prior to Miocene final breakup, and therefore before the formation of the Knipovich Ridge, again in disagreement to previous assumptions that the thermal maturities along the coasts of both margins reflect the thermal imprint of incipient seafloor spreading.

Table 2
Results of AHe Thermochronolgy

Sample		U [ppm]	Th [ppm]	Sm [ppm]	He [ncc]	TAE[a] [%]	Raw age [Ma]	eU[b] [ppm]	Rs[c] [µm]	Ft[d]	N ter[e]	Corrected age [Ma]	± error [Ma]*
	Nakkehoved–81° 44.257′N 13° 30.028′ W 137 m, Nakkehoved Fm: greywacke, Upper Cretaceous/Maastricht												
CXX-02	#1	20	4	52	0.123	1.1	37	21	50	0.68	1	55	3
CXX-03	#2	13	58	47	0.14	0.9	36	27	52	0.67	1	54	3
CXX-04	#2	3	30	58	0.08	1.2	36	10	46	0.62	2	57	3
CXX-11	Nakkehoved, 81° 43.381′ N 13° 22.676″ W 432 m, Nakkehoved Fm: greywacke, Upper Cretaceous/Maastricht												
	#2	3	23	40	0.068	1.1	37	8	49	0.65	0	57	3
	#3	4	16	45	0.033	2.5	27	8	43	0.61	0	43	2
Prinsesse Islands													
CXX-44	Prinsesse Margrethe Island, 82° 04.609′ N 17° 47.223′ W 47 m, Thyra Ø Fm: sandstone, Paleocene-Eocene												
	#5	27	6	12	0.125	0.9	21	29	50	0.67	0	31	2
	#6	76	25	50	0.176	0.9	24	82	41	0.61	1	40	2
	#7	36	9	32	0.066	1.4	20	38	47	0.66	1	30	2
	#8	35	9	25	0.105	1.1	18	37	45	0.64	0	28	1
CXX-49	Prinsesse Thyra Island, 82° 02.074′ N 19° 02.747′ W 12 m, Thyra Ø Fm: sandstone, Paleocene-Eocene												
	#3	7	27	32	0.041	2	23	14	45	0.62	1	37	2
	#4	5	14	12	0.036	2.2	23	8	46	0.64	0	37	2
	#5	3	14	20	0.028	1.7	29	7	44	0.61	0	48	3
CXX-50	Prinsesse Thyra Island, 81° 52.359′ N 19° 07.717′ W 25 m, Thyra Ø Fm: sandstone, Paleocene-Eocene												
	#4	42	397	22	1.216	0.3	19	134	63	0.72	0	27	1
	#5	22	170	20	0.391	0.6	58	62	40	0.55	0	106	5
	#6	26	131	42	0.754	0.7	64	56	46	0.62	2	103	5
	#7	54	644	46	0.804	0.5	16	204	47	0.62	2	26	1
	#8	26	253	26	0.302	1.2	17	85	46	0.63	0	27	1
Prins Karls Forland													
PKF2019-1	Reinhardpynten, 78° 33.4560′ N 11° 16.9040′ E 17 m, Sesshøgda Fm: coarse sandstone, Eocene												
	#1	30	41	58	0.071	1.5	25	39	40	0.59	1	41	2
	#2	44	38	71	0.06	1.1	15	53	40	0.59	1	25	1
PKF2019-2	Reinhardpynten, 78° 33.3680′ N 11° 16.3680′ E 10 m, Selvågen Fm: conglomerate, Eocene												
	#1	43	40	50	0.19	2.4	16	52	46	0.61	2	24	1
	#2	21	122	76	0.056	1.3	13	50	44	0.61	1	21	1
	#3	22	20	42	0.103	0.9	18	27	49	0.6	0	26	1
	#4	15	4	15	0.065	12.5	28	16	41	0.62	2	45	6
PKF2019-5	Reinhardpynten, 78° 33.4140′ N 11° 16.6030′ E 14 m, Sesshøgda Fm: coarse sandstone, Eocene												
	#1	26	46	48	0.159	0.7	19	36	43	0.66	2	31	2
	#2	50	64	40	0.201	0.8	22	65	42	0.58	0	36	2
	#3	24	18	44	0.036	2.2	20	28	41	0.68	1	33	2
PKF2019-9	Peter Winterbukta, 78° 35.5770′ N 11° 13.2710′ E 2 m, Marchaiselaguna Fm: fine sandstone, Eocene-Oligocene												
	#1	21	31	45	0.089	0.6	21	29	44	0.64	0	33	2
	#2	22	31	48	0.146	0.7	20	30	48	0.61	2	29	2
PKF2019-12	Krokodillen, 78° 35.1900′ N 11° 7.9390′ E 100 m, Selvågen Fm: conglomerate, Eocene												
	#1	9	38	21	0.038	1.4	18	17	41	0.67	0	30	2
	#2	24	60	73	0.098	0.9	14	38	53	0.62	1	21	1
PKF2019-14	Krokodillen, 78° 35.1010′ N 11° 6.7870′ E 218 m, Sesshøgda Fm: coarse sandstone, Eocene												

Table 2
Continued

Sample		U [ppm]	Th [ppm]	Sm [ppm]	He [ncc]	TAE[a] [%]	Raw age [Ma]	eU[b] [ppm]	Rs[c] [μm]	Ft[d]	N ter[e]	Corrected age [Ma]	± error [Ma]*
	#1	20	37	58	0.108	1.1	22	29	50	0.66	1	33	2
PKF2019-16	Dawespynten, 78° 32.8000′ N 11° 23.1050′ E 1 m, Reinhardpynten Fm: sandstone, Eocene-Oligocene												
	#1	17	35	39	0.231	0.6	26	25	52	0.68	2	38	2
	#2	10	20	25	0.071	1.3	32	15	42	0.61	0	51	3
	#3	20	50	53	0.093	1.2	24	31	40	0.59	0	39	2

*Ft-correction with 5% error and TAE. [a]TAE = Total analytical error. [b]eU = Effective Uranium content, calculated as eU = U + 0.235Th + 0.0053Sm. [c]Rs = Equivalent sphere radius. [d]Ft = α-ejection correction. [e]N ter = Number of terminations of the analyzed grain.

4.2. Thermal History Modeling

After complete resetting of a radiometric dating system, thermal history modeling dates the time when a sample cooled below the closure temperature but cannot record the timing of maximum heating above the closure temperature. This is why the stratigraphic ages of the analyzed sediments provide important constraints for thermal history modeling, as they bracket the timing of maximum heating between deposition and onset of cooling. For Nakkehoved, thermal history modeling narrows down a time range for the thermal event depending on which of the two depositional ages provided in the literature are included as a modeling constraint. Model 1 uses a Late Cretaceous depositional age (Håkansson et al., 1981) and yields a time range of 85 to 70 Ma for the thermal overprint. Model 2 incorporates a Maastrichtian depositional age (Svennevig et al., 2018) and provides a time range of 70 ± 5 Ma for maximum post-depositional heating. Both model solutions are in agreement with the thermochronology data. For the time period subsequent to maximum heating, both models yield concurrent time-temperature paths (Figure 4a). Relatively rapid cooling after maximum heating continued until ∼60 Ma, followed by slow cooling to surface temperatures. The samples do not record a thermal signal related to the Eurekan Orogeny. The models further allow for late Miocene cooling, which we tested in agreement with the mid-Miocene uplift recorded on the Greenland and Barents margins (Bonow & Japsen, 2021; Dörr et al., 2013; Dörr, Lisker, Piepjohn, & Spiegel, 2019; Døssing et al., 2016).

The Prinsesse Islands have experienced maximum heating at c. 50 Ma (Figure 4b) during the first stage of the Eurekan Orogeny. As for at least one sample, the AFT date was not fully reset post-deposition, the timing of heating is better constrained for the Prinsesse Island samples, as compared to the other samples of this study (under the assumptions that all Prinsesse Islands achieved maximum temperatures at the same time). In agreement with the VR data, thermal history modeling suggests higher post-depositional temperatures for the sample from Prinsesse Margrethe Island, as compared to Prinsesse Thyra Island. Subsequent to maximum heating, the models show fast to moderate cooling during the second stage of the Eurekan Orogeny, changing to slightly slower cooling rates at ∼38 Ma (i.e., similar to the end of rapid exhumation associated with the second Eurekan stage on Pearya, Vamvaka et al., 2019). Finally, the samples show slightly enhanced cooling during the Miocene, after ∼10 Ma.

For Prins Karls Forland, the thermal history models indicate post-depositional maximum heating between 45 and 35 Ma, that is, significantly later than the maximum heating of the Prinsesse Islands or Nakkehoved. Maximum heating is followed by rapid cooling during the early Oligocene, slowing down at ∼26 Ma (again similar to the end of rapid exhumation related to the post-Eurekan stage in Pearya (Vamvaka et al., 2019)). Cooling rates increase again from the late Miocene onwards, in agreement with thermal models by Blythe and Kleinspehn (1998), Dörr et al. (2012), Dörr, Lisker, Jochmann, et al. (2019), and Dörr, Lisker, Piepjohn, and Spiegel (2019). As previously mentioned, the timing of maximum heating is constrained by the stratigraphic age of the analyzed sample. For Prins Karls Forland, a depositional age during the early Eocene cannot be excluded, and in this case, maximum heating at ∼50 Ma, that is, contemporaneously with the Prinsesse Islands, would be possible. Even if this would be the case, however, both areas would differ regarding the timing of cooling through the temperature range of the fission track partial annealing zone: The samples from Prins Karls Forland start to cool below 120°C at c. 30 Ma, whereas Prinsesse Margrethe Island has already cooled to this temperature at c. 48 Ma.

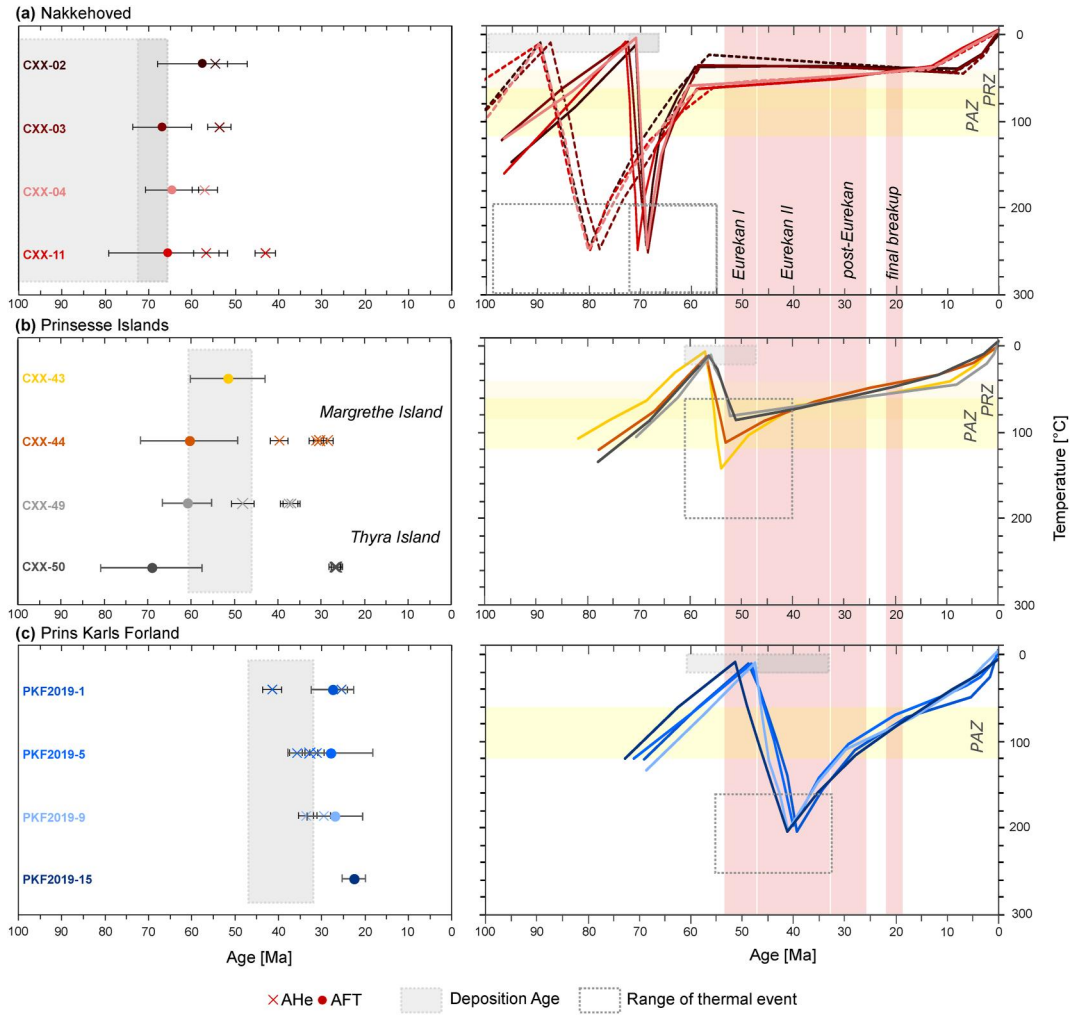

Figure 4. Visualization of AFT and AHe ages framed by the depositional ages of the sampled lithologies and results of the thermal history modeling for Nakkehoved (a), Prinsesse Islands (b) and Prins Karls Forland (c). The mean paths of the model results for the data retrieved from the sampled formations are shown. Depositional ages (cf. Figure 3) are introduced as constraining boxes in the thermal models. Further constraining boxes are the temperature range indicated by the VR data from the literature placed within the time frame between depositional age and cooling indicated by thermochronological ages (dotted lined boxes). The dotted line in (a) refers to the model incorporating a Late Cretaceous depositional age, the solid line refers to the model with a Maastrichtian depositional age.

5. Discussion

5.1. Late Cretaceous Continental Rifting Accompanied by a Shallow Thermal Anomaly

According to our thermochronology data (and also in agreement with the model of Japsen et al., 2021), heating of Nakkehoved occurred between 85 and 70 Ma. Heating was associated with temperatures of 200–300°C at depths of ~200–300 m (Håkansson et al., 1994), that is, with an (extrapolated) geothermal gradient of approximately 700°C/km. One of the few places on Earth where similar shallow thermal-gradient anomalies are observed today is the Salton Sea geothermal field, adjacent to the Gulf of California (Hulen et al., 2002; Newmark et al., 1988). Such a strong shallow thermal-gradient anomaly as observed in Nakkehoved is hard to explain by crustal extension alone and may instead be more likely related to a magmatic heat source (e.g., Lysak, 1992; Nirrengarten et al., 2020). In Kronprins Christian Land, where the Nakkehoved Formation is exposed, however, no coeval rocks of magmatic origin are known so far.

The source for magmatic heating may be located across the Atlantic Ocean on the conjugate margin. In some paleogeographic reconstructions of the Late Cretaceous to early Paleocene, Nakkehoved is located close to Bjørnøya on the Barents Shelf (Gion et al., 2017; Müller et al., 2016; Svennevig et al., 2017), adjacent to the Vestbakken Volcanic Province, a site of extensive volcanic activity. However, the earliest activity there was described as early Eocene (Faleide et al., 2010; Knutsen & Larsen, 1997; Libak et al., 2012), significantly post-dating the Late Cretaceous thermal overprint of Nakkehoved. Hence, volcanic activity in the Vestbakken Volcanic Province can be excluded as a cause of heating in Nakkehoved. Based on thermochronolgy data, Barnes and Schneider (2019) suggested a Late Cretaceous elevated geothermal gradient for the western Svalbard margin. They propose a connection to the High Arctic Large Igneous Province (HALIP), which affected large areas of the Arctic Ocean and its surrounding land masses during the Cretaceous. Even though HALIP magmatic activity makes a generally enhanced geothermal gradient in the Arctic likely, it would still not explain the extreme heat flow of the Nakkehoved area.

Alternatively, Nakkehoved may represent an allochthonous crustal fragment which was originally situated further northwest close to the magmatic centers of the Kap Washington Group volcanoes, and transported later to its current location by dextral strike-slip movements along the DGFZ. Such a scenario was already suggested by Piepjohn et al. (2016, cf. Figure 9 therein) and is further supported by the presence of a steep fault bordering the Nakkehoved basin (Døssing et al., 2010; Jokat, 2000). In this context, it is also notable that the fauna of the Nakkehoved Formation is "totally distinct from the neighboring coeval Kilen Basin" (Håkansson & Schack Pedersen, 2015, p. 165). A palinspastic reconstruction placing Nakkehoved close to the Kap Washington area of the northern coast of Greenland is illustrated in Figure 5a.

The Kap Washington Basin comprises sediments of similar age as the Nakkehoved Basin (e.g., Batten, 1982; Larsen, 1982; Manby & Lyberis, 2000; Tegner et al., 2011). The area has experienced extensive continental rift volcanism between 71 and 61 Ma (Estrada et al., 2001; Tegner et al., 2011; Thórarinsson et al., 2011). Moreover, the Kap Washington Group volcanic sequence is part of a larger magmatic province active between ∼92 and 58 Ma (Thórarinsson et al., 2011), reaching further north into the Arctic Ocean (Brotzer et al., 2022; Jokat et al., 2016), toward the east (Døssing et al., 2010), the south (Thórarinsson et al., 2015), and toward northern and western Ellesmere Island (Estrada et al., 2010; Estrada & Henjes-Kunst, 2013; Naber et al., 2021). Based on the orientation of magmatic dykes in North Greenland, at least some of this volcanic activity was associated with the break-up along the Gakkel Ridge and formation of the Eurasia Basin (Thórarinsson et al., 2015), even though actual seafloor spreading of the Gakkel Ridge only commenced during the late Paleocene/early Eocene (Schreider et al., 2019; Vogt et al., 1979).

The tectonic environment of the Kap Washington area and the Nakkehoved sedimentary basin again bears similarities with the present-day situation of the Salton Sea geothermal field: Both the Salton Sea Basin and the Kap Washington area are/were situated in a continental rift basin adjacent to a (future) oceanic spreading center associated with rhyolitic to trachytic magmatism (Estrada et al., 2001; Hulen et al., 2002; Schmitt & Hulen, 2008; Thórarinsson et al., 2011). Like the Nakkehoved Basin, the Salton Sea Basin is a pull-apart basin (Håkansson & Schack Pedersen, 2015; Hulen et al., 2002; Kaspereit et al., 2016) filled by thick syntectonic strata, which experienced greenschist-facies overprint shortly after deposition (Hulen et al., 2002; Kaspereit et al., 2016; this study). For the Salton Sea Basin, it is assumed that ascending hot brines caused the greenschist-facies metamorphism at shallow depths (Elders, 1979), and we suggest the same mechanism of hydrothermal metamorphism for the Nakkehoved Basin. In the Salton Sea geothermal system, the fluids were partly metalliferous (McKibben & Hardie, 1997), and hydrothermal alteration caused the formation of quartz, feldspar, chlorite, epidote and pyrite (Schmitt & Hulen, 2008), again similar to our observations, which include, amongst others, the growth of quartz, feldspar, chlorite, epidote, hematite, rutile, and ilmenite in the host rock and quartz veins of Nakkehoved (Supporting Information S1).

The DGFZ was already active as a dextral transform fault at the time of Kap Washington volcanism (Srivastava, 1978) and was connecting the magmatic centers of North Greenland with the rifted areas of the future Norwegian-Greenland Sea (Figure 5a). As such, the DGFZ may not only have caused displacement of the Nakkehoved crustal fragment, but may have also transported heat toward the area of the upcoming Eurekan intraplate orogeny: Transform faults are usually deeply rooted (Lee et al., 2019), and provide pathways for heat and/or fluid transport (Baietto et al., 2008; Hensen et al., 2007, 2015, 2022), particularly if they are associated with a transtensional component (Lundin et al., 2023). We speculate that heat transfer along the DGFZ caused

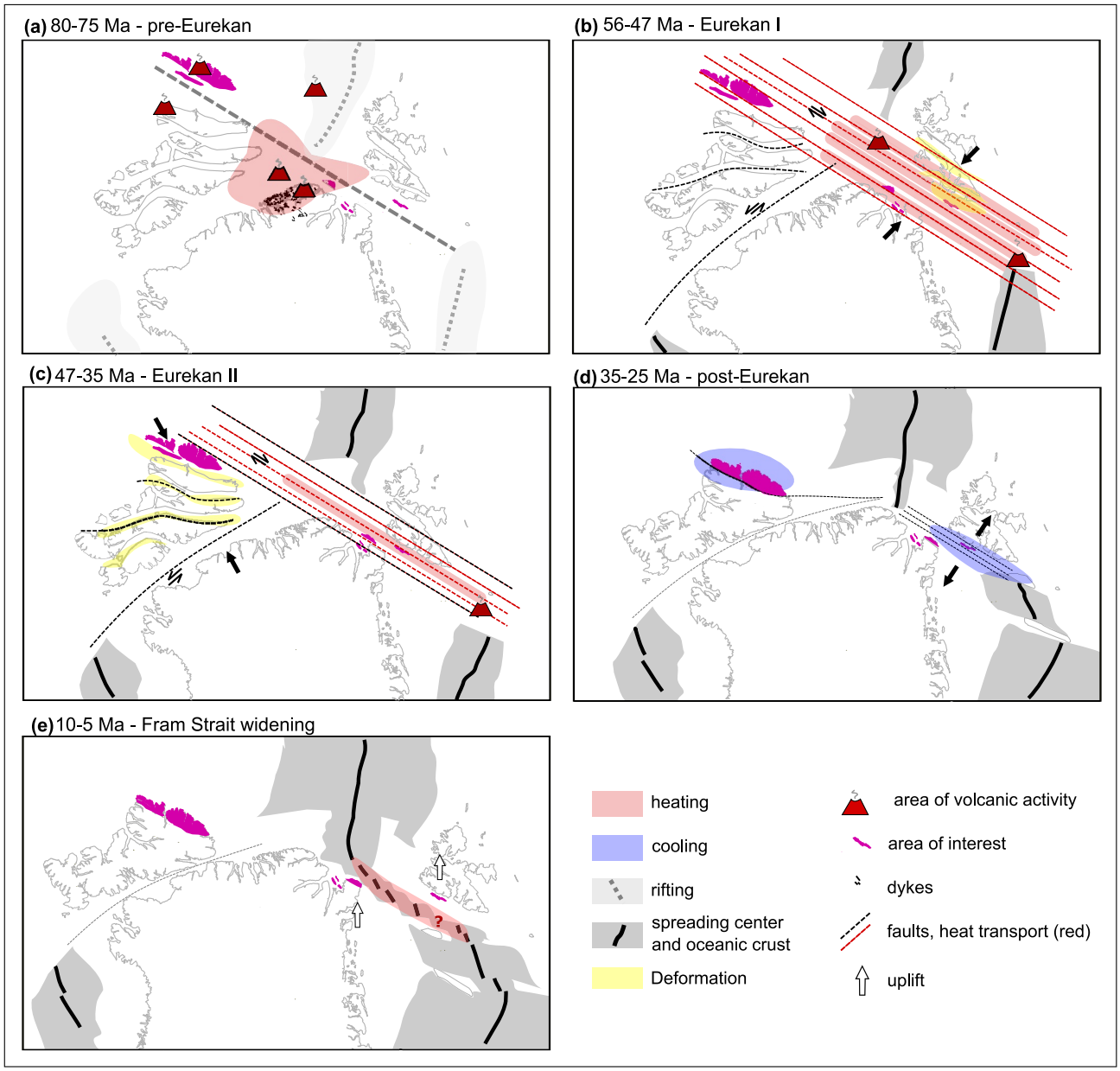

Figure 5. Schematic reconstruction of the break-up process at the conjugate margins of eastern North Greenland (a) and western Svalbard with a focus on warming and cooling episodes from the Late Cretaceous to the Late Miocene. The paleogeographic reconstruction refers to structural field data and the evolution of oceanic basins with a fixed Gakkel Ridge and is based on the work of Piepjohn et al. (2019) and Kristoffersen et al. (2020). The movement of crustal blocks is not to scale. (a) Increased heat flow and volcanic activity in the late phase of the High Arctic Large Igneous Province in the High Arctic and at Kap Washington in the Late Cretaceous (Døssing et al., 2013; Estrada et al., 2010; Estrada & Henjes-Kunst, 2004; Tegner et al., 2011; Thórarinsson et al., 2015). The crustal fragment of Nakkehoved is positioned closer to the respective heat sources and rifting in the Eurasian Basin, Norwegian-Greenland Sea and Labrador Sea/Baffin Bay area. (b) Transpessive/compressive phase of Eureka deformation at the Svalbard-Greenland margin with De Geer Fracture Zone (DGFZ) activity and onset of volcanism at the Yermak Plateau and the Vestbakken Volcanic Province in the early Eocene (Faleide et al., 2010; Piepjohn et al., 2016; Riefstahl et al., 2013). Thyra Ø Basin and the Central Tertiary Basin were heated while the geothermal gradient decreased and cooling due to inversion of fault zones occurred partially (Barnes & Schneider, 2019; Dörr, Lisker, Jochmann, et al., 2019; Japsen et al., 2021, 2023). (c) Transtensive phase of the Eurekan with progressive lateral offset and enhanced heat flow along the DGFZ. Presumably, Prins Karls Forland was heated, and the Central Tertiary Basin and potentially also the Thyra Ø Basin experienced inversion at that time (Barnes & Schneider, 2019; Dörr, Lisker, Jochmann, et al., 2019). (d) Margin-wide cooling associated with exhumation (Barnes & Schneider, 2019; Vamvaka et al., 2019) and further activity along the DGFZ. (e) Cooling phase associated with the final opening of and uplift along the Fram Strait, leading to the formation of the recent landscape (Blythe & Kleinspehn, 1998; Bonow et al., 2014; Dörr et al., 2012; Dörr, Lisker, Piepjohn, & Spiegel, 2019; Geissler et al., 2019).

localized lithospheric weak zones, which are a requirement for focusing deformation during the initial phase of intraplate orogeny (Gorczyk et al., 2012, 2013; Pysklywec & Beaumont, 2004; Raimondo et al., 2014). Accordingly, heat dissemination from HALIP magmatic activity, which ended shortly before the onset of first Eurekan movements, may have paved the way for the Eurekan intraplate orogeny, and the DGFZ may have defined its location.

5.2. The Eurekan—Heating and Cooling Along Continental Transform Faults

The Prinsesse Islands experienced maximum heating at ~50 Ma, shortly after their late Paleocene to early Eocene deposition (Lyck & Stemmerik, 2000). Maximum heating postdated heating of the Nakkehoved Basin but clearly preceded Miocene formation of the Knipovich spreading center. Our thermal history models suggest that the Prinsesse Islands experienced maximum heating at the beginning of the Eurekan Orogeny, and became involved in Eurekan deformation during an early stage of the orogeny, experiencing exhumation and erosion at least since the second stage of the Eurekan, probably earlier (Figure 4b). In agreement with published VR data, our thermochronology data indicate maximum temperatures well above ~120°C (= resetting temperature for the AFT system) for one sample from Prinsesse Margrethe Island and ~90°C (= partial resetting of the AFT system, full resetting of the AHe system) for Prinsesse Thyra Island in the west. The sedimentary basin of the Prinsesse Islands (= Thyra Ø basin) received detritus from the adjacent areas, which were exhumed in response to Eurekan tectonics. Japsen et al. (2021) found that the thickness of the Thyra Ø Formation at Kap Rigsdagen was less than 3 km based on VR and AFT data. The observed thermal maturity may hence simply be a result of burial without a thermal anomaly. However, it would require strong lateral variations in deposition rates to explain the difference in thermal maturation between Prinsesse Margrethe Island and Prinsesse Thyra Island, which are only ~20 km away from each other today. As a more likely scenario, we suggest that post-depositional heating resulted from a combination of burial and enhanced heat flow, with lateral heterogeneities regarding the distribution of heat.

Prinsesse Margrethe Island and Thyra Island are separated by a prominent fault structure (Håkansson & Schack Pedersen, 2015), and the differences between the eastern and western parts of Prinsesse Thyra Island in terms of lithification may also indicate the presence of a NW-SE striking fault. In their study on coalification in North Greenland, Paech and Estrada (2019) found differential thermal alteration in sediments present in fault zones and concluded that this may have resulted from differential conductive heat flow and deformation along the fault zones. The fault zones of the Thyra Ø basin are part of the Trolle Land Fault System and as such belong to the DGFZ. During the early Eocene, the DGFZ not only connected the incipient magmatic spreading centers of the Arctic Ocean and the Norwegian-Greenland Sea (Figure 5b), but also included the active magmatic centers of the Yermak Plateau north of Svalbard (Riefstahl et al., 2013) and of the Vestbakken Volcanic Province, the latter being a transtensional segment of the DGFZ (Faleide et al., 2010), whose activity was interpreted as "magmatic leaking" of the DGFZ (Ludin et al., 2023). Since transform faults provide an efficient transport mechanism for heat (Baietto et al., 2008; Hensen et al., 2007, 2015, 2022), the differential thermal maturation of the Prinsesse Islands likely represents an effect of activity of transform faults, imparting heat from deeply rooted sources to shallow depths and using active transform fault zones as pathways.

Prins Karls Forland is also bordered by major fault zones toward the west (Hornsund Fault Zone, part of the DGFZ) and toward the east, the latter being situated within the Forlandsundet Graben (Dallmann, 2015; Kristoffersen et al., 2020; Ritzmann et al., 2004). Heating of Prins Karls Forland occurred at or prior to ~40 Ma (Figure 4c). This is in agreement with previously published zircon fission track, Ar-Ar and zircon (U-Th)/He ages from both sedimentary rocks and the basement of Prins Karls Forland (Barnes & Schneider, 2019; Blythe & Kleinspehn, 1998; Schneider et al., 2019). At that time, the general situation was still similar to that of maximum heating of the Prinsesse Islands, with the active DGFZ connecting magmatic spreading centers in the north and in the south and the ongoing volcanic activity of the Vestbakken Volcanic Province (Figure 5c). Accordingly, we suggest that heating of Prins Karls Forland resulted from the same processes as assumed for the Prinsesse Islands, with a combination of burial and heat dissemination along the fault segment of the DGFZ.

Heating and burial of Prins Karls Forland occurred during the second stage of the Eurekan Orogeny. The comparison between the three investigated areas all situated within the DGFZ highlights the variations of transform movements during the Eurekan in terms of the vertical component. The Nakkehoved crustal fragment seems to have experienced purely lateral transport without significant vertical movements (within the sensitivity limits of low-temperature thermochronology), whereas the Prinsesse Islands of the Greenland margin and the

Prins Karls Forland of the Barents margin showed opposing vertical trends: the Prins Karls Forland experienced burial and heating, while the Prinsesse Islands were exhumed and eroded.

5.3. The Post-Eurekan Phase: Exhumation Driven by Transtension

At the end of the Eocene, seafloor spreading in the Baffin Bay/Labrador Sea area ceased and Greenland became part of the North American plate, thus ending the Eurekan Orogeny (which was defined as deformation related to movements of an independent Greenland plate; Piepjohn et al., 2016). The changed plate tectonic configuration (Srivastava & Tapscott, 1986) also induced changes in the DGFZ stress regime, which now became predominantly transtensional (Piepjohn et al., 2015). This transtensional stage was again associated with lateral and vertical movements along segments of the DGFZ/Eurekan Belt, as demonstrated for the Pearya Terrane and the West Spitsbergen Fold-and-Thrust Belt, which experienced enhanced exhumation between 34 and 26 Ma (Blythe & Kleinspehn, 1998; Vamvaka et al., 2019). At the same time, Prins Karls Forland also shows relatively rapid exhumation (Figure 4c, see also Barnes & Schneider, 2019) and a system of horst and graben structures developed along the Svalbard margin, including the formation of the Forlandsundet Graben (Blinova et al., 2009; Kleinspehn & Teyssier, 2016). Accordingly, we interpret Prins Karls Forland as a horst, which was exhumed and thus cooled during the Oligocene in response to the formation of the Forlandsundet Graben. In addition to Pearya and Prins Karls Forland, Oligocene exhumation is also described for other areas of the Arctic (Bonow et al., 2014; Bonow & Japsen, 2021; Japsen et al., 2021, 2023) (Note that Japsen et al. (2023) reported Oligocene exhumation also for the Wandel Sea Basin including Nakkehoved and the Thyra Ø Formation. It is not clear from their study whether Oligocene cooling is constraint-driven or actually required by their thermochronology data. In any case, we cannot confirm such a period of Oligocene cooling for the Wandel Sea Basin from our data).

Oligocene exhumation was not only related to tectonic denudation, but was also associated with erosional denudation, as suggested by the widespread deposition of Oligocene sediments, such as the Sarstangen Formation of the eastern Forlandsundet Graben (Eidvin et al., 1998; Kleinspehn & Teyssier, 2016; Schaaf et al., 2021), strata west of Bjørnøya (Eidvin et al., 1998) and from the Hovgård Ridge (Boulter & Manum, 1996), and presumably the Renardodden Formation (Dallmann, 2015; Livšic, 1977; Thiedig et al., 1980). The occurrence of reworked Eocene dinoflagellate cysts in these Oligocene sediments (Boulter & Manum, 1996; Eidvin et al., 1998) confirms the recycling of Eocene deposits during rapid cooling in the Oligocene. This is in agreement with our thermal history models for Prins Karls Forland, which we interpret as heating related to a combination of enhanced heat flow and burial and hence sediment deposition until ~40 Ma, followed by (erosion-related) cooling and thus removal of the Eocene sedimentary cover.

As demonstrated in this study, tectonic exhumation continued until shortly before the initiation of final continental breakup along the Fram Strait. Oligocene transtension (and related exhumation) reactivated faults that were previously active during the compressional and transpressional stages of the Eurekan Orogeny (e.g., Kristoffersen et al., 2020). Faults are zones of localized damage and act as preferred pathways for fluid and heat transport, thus causing structural weakening of the crust, as they form heterogeneities resulting from grain size reduction, generation of fracture networks, and changes of the mineral assemblage induced by fluid-rock interaction (Raimondo et al., 2014, with references). For initiating the final breakup, the Knipovich Ridge propagated toward the north along the former Eurekan Belt (Crane et al., 1988), exploiting the zones of crustal weakness inherited from the Eurekan and post-Eurekan fault movements along the DGFZ, which facilitated crustal rupture.

5.4. Final Breakup: Evolution of a Divergent Margin and the Deepening of the Fram Strait

Spreading along the Knipovich Ridge presumably initiated in the early Miocene (Dumais et al., 2020; Jokat et al., 2016). Opening and subsequent widening and deepening of the Fram Strait was related to the uplift of pre-Miocene erosion surfaces in Greenland and Svalbard (Bonow & Japsen, 2021; Dörr et al., 2013; Dörr, Lisker, Piepjohn, & Spiegel, 2019), and to the formation of a middle to late Miocene unconformity in the offshore sediments of the Greenland shelf, detected by seismic data (Døssing et al., 2016). Previous thermal history models of thermochronology data from Greenland and Svalbard also frequently involve middle or late Miocene cooling (Blythe & Kleinspehn, 1998; Dörr et al., 2013; Dörr, Lisker, Piepjohn, & Spiegel, 2019; Japsen et al., 2021, 2023), but these cooling periods are poorly constrained and differ in terms of their timing. We included Miocene cooling as a constraint in our thermal history inversions. Our models show that samples from the Greenland and Svalbard margins experienced final cooling in the late Miocene. This may be associated with a preceding, short-lived

reheating event (Figure 5e), which may be caused by enhanced heat flow associated with seafloor spreading. However, even though our models are in agreement with some Miocene heating/cooling, they do not necessarily require it for reproducing our thermochronology data. Hence, the data neither prove nor disapprove Miocene changes in the thermal regime and the thermal imprint of final continental breakup and opening of the Fram Strait remains enigmatic.

6. Conclusions

For this study, we investigated Late Cretaceous to Paleogene sedimentary rocks exposed along coastal areas on both sides of the Fram Strait. These sedimentary rocks are characterized by thermal maturation values significantly exceeding those of their neighboring sedimentary rocks of similar ages and are therefore viewed as reflecting thermal anomalies. To relate these anomalies to each other and to the plate tectonic evolution of the Fram Strait area, we analyzed the sedimentary rocks by AFT and (U-Th)/He thermochronology and reconstructed their thermal histories from Late Cretaceous rifting to final continental breakup during the Miocene:

1. Late Cretaceous deposits exposed in Nakkehoved along the Greenland margin were—largely statically heated during the latest Cretaceous, associated with an extremely high geothermal gradient and the formation of quartz veins containing feldspar, chlorite, epidote, hematite, rutile, and ilmenite. These characteristics can be compared to recent expressions of a shallow thermal anomaly associated with volcanism in the Salton Sea geothermal field. Due to the differences in terms of the thermal history and the mineralogical and faunal assemblages, we interpret the fault-bound Nakkehoved area as an allochthonous crustal fragment, which was originally situated further north in the vicinity of the Kap Washington Group volcanic centers, and which was transported to its present position by lateral movements along the DGFZ. As movements along the DGFZ were presumably also associated with heat and fluid transfer, we suggest that the activity of the DGFZ caused thermal weakening of the crust, which facilitated the formation of the Eurekan intraplate orogen.
2. Heat input into the crust via the DGFZ, connecting active volcanic centers north and south of the Fram Strait, continued during the Eocene, caused heating of the Thyra Ø Basin along the Greenland margin during the first stage of Eurekan Orogeny, and heating of Prins Karls Forland along the Barents margin during the second stage. The horizontal component associated with the lateral movements differed strongly between the different segments of the DGFZ.
3. Lateral movements of the DGFZ and associated exhumation continued post-Eurekan, caused exhumation of Prins Karls Forland during the early Oligocene, and lasted until ~26 Ma, that is, shortly before final continental breakup and initial opening of the Fram Strait. We suggest that ongoing fault activity caused further structural weakening along the DGFZ. These inherited zones of crustal weakness were exploited during the northward propagation of the Knipovich Ridge in the course of final continental breakup.
4. Our thermal history models are in agreement with an additional late Miocene cooling event associated with the deepening and widening of the Fram Strait. This cooling event, however, is not necessarily required for reproducing our thermochronology data.

All thermal and exhumational processes observed from our data can be explained by movements and heat/fluid transfer along the DGFZ. Our study adds to the growing evidence for the important role of structural inheritance and continental transform faults for continental rifting and the development of divergent continental margins.

Data Availability Statement

Details on the analytical procedure, thin section and EMP analyses, thermal history inversions as well as detailed AFT and AHe data are available in the supporting information to this manuscript. The AFT and AHe data as well as the supporting information (Meier et al., 2024) are available at zenodo.org via https://doi.org/10.5281/zenodo.10634233 with a Creative Commons Attribution 4.0 International license.

Acknowledgments
This work was funded by the German Research Foundation (DFG grants SP673/27-1 and LI745/27-1). We would like to thank the Federal Institute for Geosciences and Natural Resources (BGR) for financing and organizing the fieldwork of the CASE and PANORAMA projects in North Greenland. CASE 20 was based in Villum Research Station and we acknowledge the logistics provided by the Department of Environmental Science, Aarhus University and would like to thank the CASE 20 Team for support in the field. We would also like to thank the captain and crew of RV Polarstern cruise PS115/1, helicopter crew and wildlife observers for making fieldwork possible and Maximilian Zundel for organization and support during sample collection. Fieldwork on PKF was partly funded by ARCEx partners and the Research Council of Norway (grant 228107) and we thank captain Jan Pechar and crew Jakub and Thereza of RV Clione of the Czech Arctic Research Station of the University of South Bohemia, Rakul Johannesen for field assistance and UNIS for logistics. We are grateful for the contributions of Hans Jürgen Paech who provided maps and sample locations as well as fruitful discussion, Nikola Koglin who gave thoughts on thin sections and her expertise, Martin Blumenthal and Jolanta Kuss who gave valuable insights on the thermal maturity of associated sample material and Andreas Klügel who made the EMPA possible. We also thank Anke Toltz, Vera Kolb, Anne Hübner and Christiane Schott from the processing laboratory of the University of Bremen for technical support. Discussions with Kristian Svennevig, Winfried Dallmann, Solveig Estrada and the BGR Arctic Seminar contributed greatly to this manuscript. Furthermore, we thank three reviewers, particularly Morgan Jones and Tim Redfield for their constructive and helpful suggestions and Peter van der Beek for the editorial handling. Open Access funding enabled and organized by Projekt DEAL.

References

Baietto, A., Cadoppi, P., Martinotti, G., Perello, P., Perrochet, P., & Vuataz, F.-D. (2008). Assessment of thermal circulations in strike-slip fault systems: The Terme di Valdieri case (Italian western Alps). *Geological Society, London, Special Publications*, *299*(1), 317–339. https://doi.org/10.1144/SP299.19

Barnes, C. J., & Schneider, D. A. (2019). Late Cretaceous–Paleogene burial and exhumation history of the Southwestern Basement Province, Svalbard, revealed by zircon (U-Th)/He thermochronology. In K. Piepjohn, J. V. Strauss, L. Reinhardt, & W. C. McClelland (Eds.), *Circum-*

Arctic structural events: Tectonic evolution of the Arctic margins and trans-Arctic links with adjacent orogens (pp. 132–152). Geological Society of America. https://doi.org/10.1130/2018.2541(07

Batten, D. (1982). Palynology of shales associated with the Kap Washington Group volcanics, central North Greenland. *Rapport Grønlands Geologiske Undersøgelse*, *108*, 15–23. https://doi.org/10.34194/rapggu.v108.7778

Beucher, R., Brown, R. W., Roper, S., Stuart, F., & Persano, C. (2013). Natural age dispersion arising from the analysis of broken crystals: Part II. Practical application to apatite (U–Th)/He thermochronometry. *Geochimica et Cosmochimica Acta*, *120*, 395–416. https://doi.org/10.1016/j.gca.2013.05.042

Bjerager, M., Alsen, P., Hovikoski, J., Lindström, S., Pilgaard, A., Stemmerik, L., & Therkelsen, J. (2019). Triassic lithostratigraphy of the Wandel Sea Basin, North Greenland. *Bulletin of the Geological Society of Denmark*, *67*, 83–105. https://doi.org/10.37570/bgsd-2019-67-06

Blackwell, D. D. (1978). 8: Heat flow and energy loss in the Western United States. In *Geological society of America memoirs. Cenozoic tectonics and regional geophysics of the western Cordillera* (Vol. 152, pp. 175–208). Geological Society of America. https://doi.org/10.1130/MEM152-p175

Blinova, M., Thorsen, R., Mjelde, R., & Faleide, J. I. (2009). Structure and evolution of the Bellsund Graben between Forlandsundet and Bellsund (Spitsbergen) based on marine seismic data, *Norwegian Journal of Geology*, 89(3), 215–228. ISSN 029-196X.

Blythe, A. E., & Kleinspehn, K. L. (1998). Tectonically versus climatically driven Cenozoic exhumation of the Eurasian plate margin, Svalbard: Fission track analyses. *Tectonics*, *17*(4), 621–639. https://doi.org/10.1029/98TC01890

Bonow, J. M., & Japsen, P. (2021). Peneplains and tectonics in North-East Greenland after opening of the North-East Atlantic. *GEUS Bulletin*, *45*(1). https://doi.org/10.34194/geusb.v45.5297

Bonow, J. M., Japsen, P., & Nielsen, T. F. (2014). High-level landscapes along the margin of southern East Greenland—A record of tectonic uplift and incision after breakup in the NE Atlantic. *Global and Planetary Change*, *116*, 10–29. https://doi.org/10.1016/j.gloplacha.2014.01.010

Boulter, M. C., & Manum, S. B. (1996). Oligocene and Miocene vegetation in high latitudes of the North Atlantic: Palynological evidence from the Hovgard Ridge in the Greenland Sea (site 908). In J. Thiede, A. M. Myhre, J. V. Firth, G. L. Johnson, & W. F. Ruddiman (Eds.), *Proceedings of the scientific ocean drilling programm: Scientific results* (pp. 289–296).

Boyd, A. (1990). The Thyra Ø flora: Toward an understanding of the climate and vegetation during the early Tertiary in the High Arctic. *Review of Palaeobotany and Palynology*, *62*(3–4), 189–203. https://doi.org/10.1016/0034-6667(90)90089-2

Brott, C. A., Blackwell, D. D., & Ziagos, J. P. (1981). Thermal and tectonic implications of heat flow in the eastern Snake River Plain, Idaho. *Journal of Geophysical Research*, *86*(B12), 11709–11734. https://doi.org/10.1029/JB086iB12p11709

Brotzer, A., Funck, T., Geissler, W. H., Piepjohn, K., Heyde, I., & Berglar, K. (2022). Geophysical insights on the crustal structure of Greenland's northern continental margin towards the Morris Jesup Spur. *Tectonophysics*, *843*, 229588. https://doi.org/10.1016/j.tecto.2022.229588

Brown, R. W., Beucher, R., Roper, S., Persano, C., Stuart, F., & Fitzgerald, P. (2013). Natural age dispersion arising from the analysis of broken crystals. Part I: Theoretical basis and implications for the apatite (U–Th)/He thermochronometer. *Geochimica et Cosmochimica Acta*, *122*, 478–497. https://doi.org/10.1016/j.gca.2013.05.041

Burnham, A. K., & Sweeney, J. J. (1989). A chemical kinetic model of vitrinite maturation and reflectance. *Geochimica et Cosmochimica Acta*, *53*(10), 2649–2657. https://doi.org/10.1016/0016-7037(89)90136-1

Čepek, P. (2001). Paleogene calcareous nannofossils from the Firkanten and Sarsbukta formations on Spitsbergen. In F. Tessensohn (Ed.), *Intra-Continental Fold Belts, CASE 1: West Spitsbergen. Geologisches Jahrbuch (Polar Issue No.7)* (Vol. 91, pp. 535–547). Bundesanstalt für Geowissenschaften und Rohstoffe.

Chapman, D. S., & Rybach, L. (1985). Heat flow anomalies and their interpretation. *Journal of Geodynamics*, *4*(1–4), 3–37. https://doi.org/10.1016/0264-3707(85)90049-3

Crane, K., Sundvor, E., Foucher, J.-P., Hobart, M., Myhre, A. M., & LeDouaran, S. (1988). Thermal evolution of the western Svalbard margin. *Marine Geophysical Researches*, *9*(2), 165–194. https://doi.org/10.1007/BF00369247

Dallmann, W. K. (Ed.). (1999). *Lithostratigrafic Lexicon of Svalbard: Upper Palaeozoic to quaternary Bed Rock*. Review and recommendations for nomenclature use. Committee on the Stratigraphy of Svalbard / Norsk Polarinstitutt.

Dallmann, W. K. (Ed.). (2015). *Report Series No. 148. Geoscience atlas of spitsbergen*. Tromsø.

Dallmann, W. K. (2020). *Notes on the geology of Prins Karls Forland: Review and results of geological mapping and investigations in 2012-14*. Norsk Polarinstitutt Rapportserie; 152. Norsk Polarinstitutt. Retrieved from https://brage.npolar.no/npolar-xmlui/handle/11250/2717175

Dawes, P. R., & Soper, N. J. (1973). Pre-Quaternary history of North Greenland. In M. G. Pitcher (Ed.), *Arctic geology* (Vol. 19, pp. 117–134). American Association of Petroleum Geologists. https://doi.org/10.1306/M19375C10

Deer, W. A., Howie, R. A., & Zussman, J. (2013). *An introduction to the rock-forming minerals*. Mineralogical Society of Great Britain and Ireland.

Donelick, R. A., O'Sullivan, P. B., & Ketcham, R. A. (2005). Apatite fission-track analysis. *Reviews in Mineralogy and Geochemistry*, *58*(1), 49–94. https://doi.org/10.2138/rmg.2005.58.3

Dörr, N., Clift, P. D., Lisker, F., & Spiegel, C. (2013). Why is Svalbard an island? Evidence for two-stage uplift, magmatic underplating, and mantle thermal anomalies. *Tectonics*, *32*(3), 473–486. https://doi.org/10.1002/tect.20039

Dörr, N., Lisker, F., Clift, P. D., Carter, A., Gee, D. G., Tebenkov, A. M., & Spiegel, C. (2012). Late Mesozoic–Cenozoic exhumation history of northern Svalbard and its regional significance: Constraints from apatite fission track analysis. *Tectonophysics*, *514–517*, 81–92. https://doi.org/10.1016/j.tecto.2011.10.007

Dörr, N., Lisker, F., Jochmann, M., Rainer, T., Schlegel, A., Schubert, K., & Spiegel, C. (2019). Subsidence, rapid inversion, and slow erosion of the Central Tertiary Basin of Svalbard: Evidence from the thermal evolution and basin modeling. In K. Piepjohn, J. V. Strauss, L. Reinhardt, & W. C. McClelland (Eds.), *Circum-Arctic structural events: Tectonic evolution of the Arctic margins and trans-Arctic links with adjacent orogens* (pp. 169–188). Geological Society of America. https://doi.org/10.1130/2018.2541(09

Dörr, N., Lisker, F., Piepjohn, K., & Spiegel, C. (2019). Cenozoic development of northern Svalbard based on thermochronological data. *Terra Nova*, *31*(3), 306–315. https://doi.org/10.1111/ter.12402

Døssing, A., Dahl-Jensen, T., Thybo, H., Mjelde, R., & Nishimura, Y. (2008). East Greenland Ridge in the North Atlantic Ocean: An integrated geophysical study of a continental sliver in a boundary transform fault setting. *Journal of Geophysical Research*, *113*(B10). https://doi.org/10.1029/2007JB005536

Døssing, A., Jackson, H. R., Matzka, J., Einarsson, I., Rasmussen, T. M., Olesen, A. V., & Brozena, J. M. (2013). On the origin of the Amerasia Basin and the High Arctic Large Igneous Province—Results of new aeromagnetic data. *Earth and Planetary Science Letters*, *363*, 219–230. https://doi.org/10.1016/j.epsl.2012.12.013

Døssing, A., Japsen, P., Watts, A. B., Nielsen, T., Jokat, W., Thybo, H., & Dahl-Jensen, T. (2016). Miocene uplift of the NE Greenland margin linked to plate tectonics: Seismic evidence from the Greenland Fracture Zone, NE Atlantic. *Tectonics*, *35*(2), 257–282. https://doi.org/10.1002/2015TC004079

Døssing, A., Stemmerik, L., Dahl-Jensen, T., & Schlindwein, V. (2010). Segmentation of the eastern North Greenland oblique-shear margin—Regional plate tectonic implications. *Earth and Planetary Science Letters*, *292*(3–4), 239–253. https://doi.org/10.1016/j.epsl.2009.12.036
Dumais, M.-A., Gernigon, L., Olesen, O., Johansen, S. E., & Brönner, M. (2020). New interpretation of the spreading evolution of the Knipovich Ridge derived from aeromagnetic data. *Geophysical Journal International*, *224*(2), 1422–1428. https://doi.org/10.1093/gji/ggaa527
Eidvin, T., Goll, R. M., Grogan, P., Smelror, M., & Ulleberg, K. (1998). The Pleistocene to Middle Eocene stratigraphy and geological evolution of the western Barents Sea continental margin at well site 7316/5-1 (Bjørnøya West area). *Norsk Geologisk Tidsskrift*, *78*, 99–123.
Elders, W. A. (1979). The geological background of the geothermal fields of the Salton Trough. In *Geology and Geothermics of the Salton Trough*. (pp.1–19). Campus Museum Contributions; 5. University of California.
Engen, Ø., Faleide, J. I., & Dyreng, T. K. (2008). Opening of the Fram Strait gateway: A review of plate tectonic constraints. *Tectonophysics*, *450*(1–4), 51–69. https://doi.org/10.1016/j.tecto.2008.01.002
Estrada, S., & Henjes-Kunst, F. (2004). Volcanism in the Canadian High Arctic related to the opening of the Arctic Ocean. *Zeitschrift der Deutschen Geologischen Gesellschaft*, *154*(4), 579–603. https://doi.org/10.1127/zdgg/154/2004/579
Estrada, S., & Henjes-Kunst, F. (2013). 40Ar-39Ar and U-Pb dating of Cretaceous continental rift-related magmatism on the northeast Canadian Arctic margin. *Zeitschrift der Deutschen Gesellschaft für Geowissenschaften*, *164*(1), 107–130. https://doi.org/10.1127/1860-1804/2013/0005
Estrada, S., Henjes-Kunst, F., Melcher, F., & Tessensohn, F. (2010). Paleocene alkaline volcanism in the Nares Strait region: Evidence from volcanic pebbles. *International Journal of Earth Sciences*, *99*(4), 863–890. https://doi.org/10.1007/s00531-009-0432-6
Estrada, S., Höhndorf, A., & Henjes-Kunst, F. (2001). Cretaceous/Tertiary volcanism in North Greenland: The Kap Washington Group. *Polarforschung*, (69), 17–23.
Faleide, J. I., Bjørlykke, K., & Gabrielsen, R. H. (2010). Geology of the Norwegian continental shelf. In K. Bjorlykke (Ed.), *Petroleum geoscience* (pp. 467–499). Springer Berlin Heidelberg. https://doi.org/10.1007/978-3-642-02332-3_22
Faleide, J. I., Tsikalas, F., Breivik, A. J., Mjelde, R., Ritzmann, O., Engen, Ø., et al. (2008). Structure and evolution of the continental margin off Norway and the Barents Sea. *Episodes*, *31*(1), 82–91. https://doi.org/10.18814/epiiugs/2008/v31i1/012
Faleide, J. I., Vågnes, E., & Gudlaugsson, S. T. (1993). Late Mesozoic-Cenozoic evolution of the south-western Barents Sea in a regional rift-shear tectonic setting. *Marine and Petroleum Geology*, *10*(3), 186–214. https://doi.org/10.1016/0264-8172(93)90104-Z
Farley, K. A. (2000). Helium diffusion from apatite: General behavior as illustrated by Durango fluorapatite. *Journal of Geophysical Research*, *105*(B2), 2903–2914. https://doi.org/10.1029/1999JB900348
Farley, K. A. (2002). (U-Th)/He dating: Techniques, calibrations, and applications. *Reviews in Mineralogy and Geochemistry*, *47*(1), 819–844. https://doi.org/10.2138/rmg.2002.47.18
Farley, K. A., Wolf, R. A., & Silver, L. T. (1996). The effects of long alpha-stopping distances on (U-Th)/He ages. *Geochimica et Cosmochimica Acta*, *60*(21), 4223–4229. https://doi.org/10.1016/S0016-7037(96)00193-7
Flowers, R. M., Ketcham, R. A., Shuster, D. L., & Farley, K. A. (2009). Apatite (U–Th)/He thermochronometry using a radiation damage accumulation and annealing model. *Geochimica et Cosmochimica Acta*, *73*(8), 2347–2365. https://doi.org/10.1016/j.gca.2009.01.015
Frebold, H. (1935). Geologie von Spitzbergen, der Bäreninseln, des König Karl-und Franz-Joseph-Landes. In E. Krenkel (Ed.), *Geologie der Erde* (pp. 1–195). Gebrüder Borntraeger.
Gabrielsen, R. H., Faerseth, R. B., Jensen, L. N., Kalheim, J. E., & Riis, F. (1990). *Structural elements of the Norwegian continental shelf: Part 1, the Barents sea region*. Norwegian Petroleum Directorate Bulletin, 6.
Gabrielsen, R. H., Kløvjan, O. S., Haugsbø, H., Midbøe, P. S., Nøttvedt, A., Rasmussen, E., & Skott, P. H. (1992). A structural outline of Forlandsundet Graben, Prins Karls Forland, Svalbard. *Norsk Geologisk Tidsskrift*, (72), 105–120.
Geissler, W. H., Estrada, S., Riefstahl, F., O'Connor, J. M., Spiegel, C., van den Boogard, P., & Klügel, A. (2019). Middle Miocene magmatic activity in the Sophia basin, Arctic Ocean—Evidence from dredged basalt at the flanks of Mosby Seamount. *Arktos*, *5*(1), 31–48. https://doi.org/10.1007/s41063-019-00066-8
Gernigon, L., Gaina, C., Olesen, O., Ball, P. J., Péron-Pinvidic, G., & Yamasaki, T. (2012). The Norway Basin revisited: From continental breakup to spreading ridge extinction. *Marine and Petroleum Geology*, *35*(1), 1–19. https://doi.org/10.1016/j.marpetgeo.2012.02.015
Gion, A. M., Williams, S. E., & Müller, R. D. (2017). A reconstruction of the Eurekan Orogeny incorporating deformation constraints. *Tectonics*, *36*(2), 304–320. https://doi.org/10.1002/2015TC004094
Gorczyk, W., Hobbs, B., & Gerya, T. (2012). Initiation of Rayleigh–Taylor instabilities in intra-cratonic settings. *Tectonophysics*, *514–517*, 146–155. https://doi.org/10.1016/j.tecto.2011.10.016
Gorczyk, W., Hobbs, B., Gessner, K., & Gerya, T. (2013). Intracratonic geodynamics. *Gondwana Research*, *24*(3–4), 838–848. https://doi.org/10.1016/j.gr.2013.01.006
Håkansson, E., Heinberg, C., & Stemmerik, L. (1981). The Wandel Sea Basin from Holm Land to Lockwood Ø, eastern North Greenland. *Rapport Grønlands Geologiske Undersøgelse*, *106*, 47–63. https://doi.org/10.34194/rapggu.v106.7766
Håkansson, E., Heinberg, C., & Stemmerik, L. (1991). Mesozoic and Cenozoic history of the Wandel Sea Basin area, North Greenland. *Bulletin Grønlands Geologiske Undersøgelse*, *160*, 153–164. https://doi.org/10.34194/bullggu.v160.6716
Håkansson, E., & Pedersen, S. (2001). The Wandel Hav Strike-Slip Mobile Belt – A Mesozoic plate boundary in North Greenland. *Bulletin of the Geological Society of Denmark*, *48*, 149–158. https://doi.org/10.37570/bgsd-2001-48-08
Håkansson, E., Piasecki, S., Konnerub-Madsen, J., Springer, N., & Thomse, E. (1994). A late, thermal event in the Wandel Sea Basin; eastern North Greenland. In E. Håkansson (Ed.), *Wandel Sea Basin: Basin analysis* (p. 13).
Håkansson, E., & Schack Pedersen, S. A. (1982). Late Paleozoic to Tertiary tectonic evolution of the continental margin in North Greenland. In A. E. Embry & H. R. Balkwill (Eds.), *Memoirs: Vol. 8. Arctic geology and geophysics* (pp. 331–348).
Håkansson, E., & Schack Pedersen, S. A. (2015). A healed strike-slip plate boundary in North Greenland indicated through associated pull-apart basins. In G. M. Gibson, F. Roure, & G. Manatschal (Eds.), *Special publications: Vol. 413. Sedimentary basins and crustal processes at continental margins: From modern hyper-extended margins to deformed ancient analogues* (pp. 143–169). https://doi.org/10.1144/SP413.10
Harland, W. B. (1969). Contribution of Spitsbergen to understanding of tectonic evolution of North Atlantic region. In M. Kay (Ed.), *North Atlantic—geology and continental drift* (pp. 817–851). American Association of Petroleum Geologists. https://doi.org/10.1306/M12367C58
Harland, W. B. (Ed.). (1997). The geology of Svalbard *Memoir* (Vol. 17). The Geological Society London.
Härtel, B., Jonckheere, R., Krause, J., & Ratschbacher, L. (2022). Spurious age-eU associations in thermochronological data. *Earth and Planetary Science Letters*, *599*, 117870. https://doi.org/10.1016/j.epsl.2022.117870
Hasebe, N., Barbarand, J., Jarvis, K., Carter, A., & Hurford, A. J. (2004). Apatite fission-track chronometry using laser ablation ICP-MS. *Chemical Geology*, *207*(3–4), 135–145. https://doi.org/10.1016/j.chemgeo.2004.01.007
Hensen, C., Nuzzo, M., Hornibrook, E., Pinheiro, L. M., Bock, B., Magalhães, V. H., & Brückmann, W. (2007). Sources of mud volcano fluids in the Gulf of Cadiz—Indications for hydrothermal imprint. *Geochimica et Cosmochimica Acta*, *71*(5), 1232–1248. https://doi.org/10.1016/j.gca.2006.11.022

Hensen, C., Scholz, F., Liebetrau, V., Kaul, N., Nuzzo, M., Schmidt, M., et al. (2022). Oceanic strike-slip faults represent active fluid conduits in the abyssal sub-seafloor. *Geology*, *50*(2), 189–193. https://doi.org/10.1130/G49344.1

Hensen, C., Scholz, F., Nuzzo, M., Valadares, V., Gràcia, E., Terrinha, P., et al. (2015). Strike-slip faults mediate the rise of crustal-derived fluids and mud volcanism in the deep sea. *Geology*, *43*(4), 339–342. https://doi.org/10.1130/G36359.1

Higgins, A., Friderichsen, J., & Soper, N. (1981). The North Greenland fold belt between central Johannes V. Jensen Land and eastern Nansen Land. *Rapport Grønlands Geologiske Undersøgelse*, *106*, 35–45. https://doi.org/10.34194/rapggu.v106.7765

Hovikoski, J., Pedersen, G. K., Alsen, P., Lauridsen, B. W., Svennevig, K., Nøhr-Hansen, H., et al. (2018). The Jurassic–Cretaceous lithostratigraphy of Kilen, Kronprins Christian Land, eastern North Greenland. *Bulletin of the Geological Society of Denmark*, *66*, 61–112. https://doi.org/10.37570/bgsd-2018-66-04

Huismans, R. S., & Beaumont, C. (2008). Complex rifted continental margins explained by dynamical models of depth-dependent lithospheric extension. *Geology*, *36*(2), 163. https://doi.org/10.1130/G24231A.1

Hulen, J. B., Kaspereit, D., Norton, D. L., Osborn, W., & Pulka Fred, S. (2002). *Refined conceptual modeling and a new resource estimate for the Salton Sea geothermal field, Imperial Valley, California*. Geothermal Resources Council Transactions. (26).

Hurford, A. J., & Green, P. F. (1983). The zeta age calibration of fission-track dating. *Chemical Geology*, *41*, 285–317. https://doi.org/10.1016/S0009-2541(83)80026-6

Japsen, P., Green, P. F., & Chalmers, J. A. (2021). Thermo-tectonic development of the Wandel Sea Basin, North Greenland. *GEUS Bulletin*, *45*(1). https://doi.org/10.34194/geusb.v45.5298

Japsen, P., Green, P. F., & Chalmers, J. A. (2023). Synchronous exhumation episodes across Arctic Canada, North Greenland and Svalbard in relation to the Eurekan Orogeny. *Gondwana Research*, *117*, 207–229. https://doi.org/10.1016/j.gr.2023.01.011

Jokat, W. (2000). The sediment distribution below the North Greenland continental margin and the adjacent Lena Trough. *Polarforschung*, *68*(1998), 71–82.

Jokat, W., Lehmann, P., Damaske, D., & Bradley Nelson, J. (2016). Magnetic signature of North-East Greenland, the Morris Jesup Rise, the Yermak Plateau, the central Fram Strait: Constraints for the rift/drift history between Greenland and Svalbard since the Eocene. *Tectonophysics*, *691*, 98–109. https://doi.org/10.1016/j.tecto.2015.12.002

Jones, M. T., Eliassen, G. T., Shephard, G. E., Svensen, H. H., Jochmann, M., Friis, B., et al. (2016). Provenance of bentonite layers in the Palaeocene strata of the Central Basin, Svalbard: Implications for magmatism and rifting events around the onset of the North Atlantic Igneous Province. *Journal of Volcanology and Geothermal Research*, *327*, 571–584. https://doi.org/10.1016/j.jvolgeores.2016.09.014

Kaspereit, D., Mann, M., Sanyal, S., Rickard, B., Osborn, W., & Hulen, J. B. (2016). *Updated Conceptual model and reserve estimate for the Salton Sea geothermal field, Imperial Valley, California*. Geothermal Resources Council Transactions. (40).

Ketcham, R. A. (2005). Forward and inverse modeling of low-temperature thermochronometry data. *Reviews in Mineralogy and Geochemistry*, *58*(1), 275–314. https://doi.org/10.2138/rmg.2005.58.11

Ketcham, R. A., Carter, A., Donelick, R. A., Barbarand, J., & Hurford, A. J. (2007a). Improved measurement of fission-track annealing in apatite using c-axis projection. *American Mineralogist*, *92*(5–6), 789–798. https://doi.org/10.2138/am.2007.2280

Ketcham, R. A., Carter, A., Donelick, R. A., Barbarand, J., & Hurford, A. J. (2007b). Improved modeling of fission-track annealing in apatite. *American Mineralogist*, *92*(5–6), 799–810. https://doi.org/10.2138/am.2007.2281

Ketcham, R. A., Gautheron, C., & Tassan-Got, L. (2011). Accounting for long alpha-particle stopping distances in (U–Th–Sm)/He geochronology: Refinement of the baseline case. *Geochimica et Cosmochimica Acta*, *75*(24), 7779–7791. https://doi.org/10.1016/j.gca.2011.10.011

Kleinspehn, K. L., & Teyssier, C. (1992). Tectonics of the Palaeogene Forlandsundet Basin, Spitsbergen: A preliminary report. *Geologisk Tidsskrift*, *72*(1), 93–104.

Kleinspehn, K. L., & Teyssier, C. (2016). Oblique rifting and the late Eocene–Oligocene demise of Laurasia with inception of Molloy Ridge: Deformation of Forlandsundet Basin, Svalbard. *Tectonophysics*, *693*, 363–377. https://doi.org/10.1016/j.tecto.2016.05.010

Knutsen, S.-M., & Larsen, K. I. (1997). The late Mesozoic and Cenozoic evolution of the Sørvestsnaget Basin: A tectonostratigraphic mirror for regional events along the southwestern Barents Sea margin? *Marine and Petroleum Geology*, *14*(1), 27–54. https://doi.org/10.1016/S0264-8172(96)00039-6

Kristoffersen, Y., Ohta, Y., & Hall, J. K. (2020). On the origin of the Yermak Plateau north of Svalbard, Arctic Ocean. *Norwegian Journal of Geology*, 100(1), 133. https://doi.org/10.17850/njg100-1-5

Krutzsch, W. (2001). An Upper Cretaceous microflora from Spitsbergen. In F. Tessensohn (Ed.), *Intra-Continental Fold Belts, CASE 1: West Spitsbergen. Geologisches Jahrbuch (Polar Issue No.7)* (Vol. 91, pp. 693–713). Bundesanstalt für Geowissenschaften und Rohstoffe.

Larsen, O. (1982). The age of the Kap Washington Group volcanics, North Greenland. *Bulletin of the Geological Society of Denmark*, *31*(31), 49–55. https://doi.org/10.37570/bgsd-1982-31-04

Lasabuda, A. P., Johansen, N. S., Laberg, J. S., Faleide, J. I., Senger, K., Rydningen, T. A., et al. (2021). Cenozoic uplift and erosion of the Norwegian Barents Shelf – A review. *Earth-Science Reviews*, *217*, 103609. https://doi.org/10.1016/j.earscirev.2021.103609

Lee, H., Kim, H., Kagoshima, T., Park, J.-O., Takahata, N., & Sano, Y. (2019). Mantle degassing along strike-slip faults in the Southeastern Korean Peninsula. *Scientific Reports*, *9*(1), 15334. https://doi.org/10.1038/s41598-019-51719-3

Libak, A., Mjelde, R., Keers, H., Faleide, J. I., & Murai, Y. (2012). An integrated geophysical study of Vestbakken Volcanic Province, western Barents Sea continental margin, and adjacent oceanic crust. *Marine Geophysical Researches*, *33*(2), 185–207. https://doi.org/10.1007/s11001-012-9155-3

Livšic, J. J. (1974). *Palaeogene deposits and the platform structure of Svalbard*. Norsk Polarinstitutt Skrifter, 159.

Livšic, J. J. (1977). Tertiary deposits in the western part of the Spitsbergen archipelago. In V. N. Sokolov (Ed.), *Stratigraphy of Spitsbergen* (pp.235–259). British Library Lending Division.

Livšic, J. J. (1992). Tectonic history of Tertiary sedimentation of Svalbard. *Norsk Geologisk Tidsskrift*, *72*, 121–127.

Lundin, E. R., Doré, A. G., Naliboff, J., & van Wijk, J. (2023). Utilization of continental transforms in break-up: Observations, models, and a potential link to magmatism. *Geological Society, London, Special Publications*, *524*(1), 121–145. https://doi.org/10.1144/SP524-2021-119

Lyck, J. M., & Stemmerik, L. (2000). Palynology and depositional history of the Paleocene? Thyra Ø Formation, Wandel Sea Basin, eastern North Greenland. *Geology of Greenland Survey Bulletin*, *187*, 21–49. https://doi.org/10.34194/ggub.v187.5193

Lysak, S. V. (1992). Heat flow variations in continental rifts. *Tectonophysics*, *208*(1–3), 309–323. https://doi.org/10.1016/0040-1951(92)90352-7

Manby, G., & Lyberis, N. (2000). Pre-ocean opening compression of the northwestern Atlantic margin: Evidence from eastern North Greenland. *Journal of the Geological Society*, *157*(4), 707–710. https://doi.org/10.1144/jgs.157.4.707

Manum, S. B., & Throndsen, T. (1986). Age of Tertiary formations on Spitsbergen. *Polar Research*, *4*(2), 103–131. https://doi.org/10.3402/polar.v4i2.6927

McKibben, M. A., & Hardie, L. A. (1997). Ore-forming brines in active continental rifts. *Geochemistry of Hydrothermal Ore Solutions*, *3*, 877–935.

Meier, K., O'Sullivan, P., Jochmann, M. M., Wallrath, T., Monien, P., Piepjohn, K., et al. (2024). Shallow thermal anomalies and their role in the breakup evolution along the conjugate margins of the Fram Strait (Svalbard and eastern North Greenland), indicated by low-temperature thermochronology [Dataset]. *Zenodo*. https://doi.org/10.5281/zenodo.10634233

Mosar, J., Eide, E. A., Osmundsen, P. T., Sommaruga, A., & Torsvik, T. H. (2002). Greenland-Norway separation: A geodynamic model for the North Atlantic. *Norwegian Journal of Geology*, *83*, 282–299.

Müller, R. D., Seton, M., Zahirovic, S., Williams, S. E., Matthews, K. J., Wright, N. M., et al. (2016). Ocean basin evolution and global-scale plate reorganization events since Pangea breakup. *Annual Review of Earth and Planetary Sciences*, *44*(1), 107–138. https://doi.org/10.1146/annurev-earth-060115-012211

Naber, T. V., Grasby, S. E., Cuthbertson, J. P., Rayner, N., & Tegner, C. (2021). New constraints on the age, geochemistry, and environmental impact of High Arctic Large Igneous Province magmatism: Tracing the extension of the Alpha Ridge onto Ellesmere island, Canada. *GSA Bulletin*, *133*(7–8), 1695–1711. https://doi.org/10.1130/B35792.1

Nemčok, M. (2016). The role of pre-rift heat flow in thermal regimes of rifts and passive margins. In M. Nemčok (Ed.), *Rifts and passive margins* (pp. 245–255). Cambridge University Press. https://doi.org/10.1017/CBO9781139198844.010

Newmark, R. L., Kasameyer, P. W., & Younker, L. W. (1988). Shallow drilling in the Salton Sea region: The thermal anomaly. *Journal of Geophysical Research*, *93*(B11), 13005–13023. https://doi.org/10.1029/JB093iB11p13005

Nielsen, S. B., Clausen, O. R., & McGregor, E. (2017). basin%Ro: A vitrinite reflectance model derived from basin and laboratory data. *Basin Research*, *29*(S1), 515–536. https://doi.org/10.1111/bre.12160

Nirrengarten, M., Mohn, G., Schito, A., Corrado, S., Gutiérrez-García, L., Bowden, S. A., & Despinois, F. (2020). The thermal imprint of continental breakup during the formation of the South China Sea. *Earth and Planetary Science Letters*, *531*, 115972. https://doi.org/10.1016/j.epsl.2019.115972

Oakey, G. N., & Chalmers, J. A. (2012). A new model for the Paleogene motion of Greenland relative to North America: Plate reconstructions of the Davis Strait and Nares Strait regions between Canada and Greenland. *Journal of Geophysical Research*, *117*(B10). https://doi.org/10.1029/2011JB008942

Orvin, A. K. (1940). Outline of the geological history of Spitsbergen. *Skrifter om Svalbard og Ishavet*, *78*, 1–57.

Paech, H.-J., & Estrada, S. (2019). Coal rank data and tectonic structure of Mesozoic and Paleogene sediments in North Greenland. In K. Piepjohn, J. V. Strauss, L. Reinhardt, & W. C. McClelland (Eds.), *Circum-Arctic structural events: Tectonic evolution of the Arctic margins and trans-Arctic links with adjacent orogens* (pp. 189–211). Geological Society of America. https://doi.org/10.1130/2018.2541(10

Paech, H.-J., & Koch, J. (2001). Coalification in post-Caledonian sediments on Spitsbergen. In F. Tessensohn (Ed.), *Intra-Continental Fold Belts, CASE 1: West Spitsbergen*. Geologisches Jahrbuch (Polar Issue No.7) (Vol. 91, pp. 507–530). Bundesanstalt für Geowissenschaften und Rohstoffe.

Pedersen, G. K., Lauridsen, B. W., Svennevig, K., Bojesen-Koefoed, J. A., Nøhr-Hansen, H., & Alsen, P. (2018). Burial history of a folded Cretaceous succession – A case study from the southern part of Kilen, eastern North Greenland. *Cretaceous Research*, *89*, 22–35. https://doi.org/10.1016/j.cretres.2018.03.007

Peron-Pinvidic, G., & Manatschal, G. (2019). Rifted margins: State of the art and future challenges. *Frontiers in Earth Science*, *7*. https://doi.org/10.3389/feart.2019.00218

Piasecki, S., Nøhr-Hansen, H., & Dalhoff, F. (2018). Revised stratigraphy of Kap Rigsdagen beds, Wandel Sea Basin, North Greenland. *Newsletters on Stratigraphy*, *51*(4), 411–425. https://doi.org/10.1127/nos/2018/0444

Piepjohn, K., von Gosen, W., Reinhardt, L., & Shephard, G. E. (2019). The Eurekan deformation – A reconstruction of the Cenozoic deformation in the Arctic based on geological and structural field data and observations. *AGU chapman conference on large-scale volcanism in the Arctic: The role of the mantle and tectonics, selfoss, Iceland*.

Piepjohn, K., von Gosen, W., & Tessensohn, F. (2016). The Eurekan deformation in the Arctic: An outline. *Journal of the Geological Society*, *173*(6), 1007–1024. https://doi.org/10.1144/jgs2016-081

Piepjohn, K., von Gosen, W., Tessensohn, F., Reinhardt, L., McClelland, W. C., Dallmann, W., et al. (2015). Tectonic map of the Ellesmerian and Eurekan deformation belts on Svalbard, North Greenland, and the Queen Elizabeth Islands (Canadian Arctic). *Arktos*, *1*(1), 12. https://doi.org/10.1007/s41063-015-0015-7

Prestvik, T. (1978). *Cenozoic plateau lavas of Spitsbergen–A geochemical study*. Årbok 1977.

Pysklywec, R. N., & Beaumont, C. (2004). Intraplate tectonics: Feedback between radioactive thermal weakening and crustal deformation driven by mantle lithosphere instabilities. *Earth and Planetary Science Letters*, *221*(1–4), 275–292. https://doi.org/10.1016/S0012-821X(04)00098-6

Raimondo, T., Hand, M., & Collins, W. J. (2014). Compressional intracontinental orogens: Ancient and modern perspectives. *Earth-Science Reviews*, *130*, 128–153. https://doi.org/10.1016/j.earscirev.2013.11.009

Riefstahl, F., Estrada, S., Geissler, W. H., Jokat, W., Stein, R., Kämpf, H., et al. (2013). Provenance and characteristics of rocks from the Yermak Plateau, Arctic Ocean: Petrographic, geochemical and geochronological constraints. *Marine Geology*, *343*, 125–145. https://doi.org/10.1016/j.margeo.2013.06.009

Ritzmann, O., Jokat, W., Czuba, W., Guterch, A., Mjelde, R., & Nishimura, Y. (2004). A deep seismic transect from Hovgård Ridge to northwestern Svalbard across the continental-ocean transition: A sheared margin study. *Geophysical Journal International*, *157*(2), 683–702. https://doi.org/10.1111/j.1365-246X.2004.02204.x

Ryseth, A., Auguston, J. H., Charnok, M., Haugeru, O., Knutsen, S.-M., Midbøe, P. S., et al. (2003). Cenozoic stratigraphy and evolution of the Søvestsnaget Basin, southwestern Barents Sea. *Norwegian Journal of Geology*, *83*, 107–130.

Schaaf, N. W., Osmundsen, P. T., van der Lelij, R., Schönenberger, J., Lenz, O. K., Redfield, T., & Senger, K. (2021). Tectono-sedimentary evolution of the eastern Forlandsundet Graben, Svalbard. *Norwegian Journal of Geology*, 100(4), 1–39. https://doi.org/10.17850/njg100–4–4

Schmitt, A. K., & Hulen, J. B. (2008). Buried rhyolites within the active, high-temperature Salton Sea geothermal system. *Journal of Volcanology and Geothermal Research*, *178*(4), 708–718. https://doi.org/10.1016/j.jvolgeores.2008.09.001

Schneider, D. A., Faehnrich, K., Majka, J., & Manecki, M. (2019). 40Ar/39Ar geochronologic evidence of Eurekan deformation within the West Spitsbergen Fold and Thrust Belt. In K. Piepjohn, J. V. Strauss, L. Reinhardt, & W. C. McClelland (Eds.), *Circum-Arctic structural events: Tectonic evolution of the Arctic margins and trans-Arctic links with adjacent orogens* (pp. 153–168). Geological Society of America. https://doi.org/10.1130/2018.2541(08

Schreider, A. A., Schreider, A. A., Sazhneva, A. E., Kluev, M. S., & Brehovskih, A. L. (2019). Kinematic model of development of eastern areas of the Gakkel mid-ocean ridge in the Eurasian Basin of the Arctic Ocean. *Oceanology*, *59*(1), 133–142. https://doi.org/10.1134/S0001437019010193

Senger, K., Tveranger, J., Ogata, K., Braathen, A., & Planke, S. (2014). Late Mesozoic magmatism in Svalbard: A review. *Earth-Science Reviews*, *139*, 123–144. https://doi.org/10.1016/j.earscirev.2014.09.002

Shuster, D. L., Flowers, R. M., & Farley, K. A. (2006). The influence of natural radiation damage on helium diffusion kinetics in apatite. *Earth and Planetary Science Letters*, *249*(3–4), 148–161. https://doi.org/10.1016/j.epsl.2006.07.028

Smelror, M., & Larssen, G. B. (2016). Are there Upper Cretaceous sedimentary rocks preserved on Sørkapp Land, Svalbard? *Norwegian Journal of Geology*, 96(2), 147–158. https://doi.org/10.17850/njg96-2-05

Soper, N. J., & Higgins, A. K. (1987). A shallow detachment beneath the North Greenland fold belt: Implications for sedimentation and tectonics. *Geological Magazine*, *124*(5), 441–450. https://doi.org/10.1017/S0016756800017027

Soper, N. J., & Higgins, A. K. (1991). Late Cretaceous – Early Tertiary deformation, North Greenland. In H. P. Trettin (Ed.), *Geology of the Innuitian Orogen and Arctic Platform of Canada and Greenland* (pp. 459–465). Geological Society of America. https://doi.org/10.1130/DNAG-GNA-E.467

Spiegel, C., Kohn, B., Belton, D., Berner, Z., & Gleadow, A. (2009). Apatite (U–Th–Sm)/He thermochronology of rapidly cooled samples: The effect of He implantation. *Earth and Planetary Science Letters*, *285*(1–2), 105–114. https://doi.org/10.1016/j.epsl.2009.05.045

Srivastava, S. P. (1978). Evolution of the Labrador Sea and its bearing on the early evolution of the North Atlantic. *Geophysical Journal International*, *52*(2), 313–357. https://doi.org/10.1111/j.1365-246X.1978.tb04235.x

Srivastava, S. P., & Tapscott, C. R. (1986). Plate kinematics of the North Atlantic. In P. R. Vogt & B. E. Tucholke (Eds.), *The western North Atlantic region* (pp. 379–404). North America: Geology of North America. https://doi.org/10.1130/DNAG-GNA-M.379

Sushchevskaya, N. M., Korago, E. A., Belyatsky, B. V., & Sirotkin, A. N. (2009). Geochemistry of Neogene magmatism at Spitsbergen island. *Geochemistry International*, *47*(10), 966–978. https://doi.org/10.1134/S0016702909100024

Svennevig, K., Alsen, P., & Guarnieri, P. (2018). Descriptive text to the geological map of Greenland, 1:100 000, Kilen 81 Ø.1 Syd. *Geological survey of Denmark and Greenland map series: 8 (2018)*. GEUS.

Svennevig, K., Guarnieri, P., & Stemmerik, L. (2016). Tectonic inversion in the Wandel Sea Basin: A new structural model of Kilen (eastern North Greenland). *Tectonics*, *35*(12), 2896–2917. https://doi.org/10.1002/2016TC004152

Svennevig, K., Guarnieri, P., & Stemmerik, L. (2017). 3D restoration of a Cretaceous rift basin in Kilen, eastern North Greenland. *Norwegian Journal of Geology*, *99*(1), 21–32. https://doi.org/10.17850/njg97-1-02

Talwani, M., & Eldholm, O. (1977). Evolution of the Norwegian-Greenland Sea. *GSA Bulletin*, *88*(7), 969. https://doi.org/10.1130/0016-7606(1977)88%3C969:EOTNS%3E2.0.CO;2

Tegner, C., Storey, M., Holm, P. M., Thorarinsson, S. B., Zhao, X., Lo, C.-H., & Knudsen, M. F. (2011). Magmatism and Eurekan deformation in the High Arctic Large Igneous Province: 40Ar–39Ar age of Kap Washington Group volcanics, North Greenland. *Earth and Planetary Science Letters*, *303*(3–4), 203–214. https://doi.org/10.1016/j.epsl.2010.12.047

Thiedig, F., Pickton, C. A. G., Lehmann, U., Harland, W. B., & Anderson, H. J. (1980). Das Tertiär von Renardodden (Ostlich Kapp Lyell, Westspitzbergen, Svalbard). *Mitteilungen aus dem Geologisch-Palaontologischen Institut der Universitat Hamburg*, *49*, 135–146.

Thórarinsson, S. B., Holm, P. M., Tappe, S., Heaman, L. M., & Tegner, C. (2011). Late Cretaceous–Palaeocene continental rifting in the High Arctic: U–Pb geochronology of the Kap Washington Group volcanic sequence, North Greenland. *Journal of the Geological Society*, *168*(5), 1093–1106. https://doi.org/10.1144/0016-76492011-018

Thórarinsson, S. B., Söderlund, U., Døssing, A., Holm, P. M., Ernst, R. E., & Tegner, C. (2015). Rift magmatism on the Eurasia Basin margin: U–Pb baddeleyite ages of alkaline dyke swarms in North Greenland. *Journal of the Geological Society*, *172*(6), 721–726. https://doi.org/10.1144/jgs2015-049

Thorsteinsson, R., & Tozer, E. T. (1970). Geology of the Arctic archipelago. In R. Douglass (Ed.), *Economic geology report* (Vol. 1, pp. 547–590). Geology and Economic Minerals of Canada.

Vamvaka, A., Pross, J., Monien, P., Piepjohn, K., Estrada, S., Lisker, F., & Spiegel, C. (2019). Exhuming the top end of North America: Episodic evolution of the Eurekan belt and its potential relationships to north Atlantic plate tectonics and Arctic climate change. *Tectonics*, *38*(12), 4207–4228. https://doi.org/10.1029/2019TC005621

Vermeesch, P. (2018). IsoplotR: A free and open toolbox for geochronology. *Geoscience Frontiers*, *9*(5), 1479–1493. https://doi.org/10.1016/j.gsf.2018.04.001

Vogt, P. R., Taylor, P. T., Kovacs, L. C., & Johnson, G. L. (1979). Detailed aeromagnetic investigation of the Arctic Basin. *Journal of Geophysical Research*, *84*(B3), 1071–1089. https://doi.org/10.1029/JB084iB03p01071

von Gosen, W., & Piepjohn, K. (2003). Eurekan transpressive deformation in the Wandel Hav Mobile Belt (northeast Greenland). *Tectonics*, *22*(4), 13–28. https://doi.org/10.1029/2001TC901040

Wagner, G. A., Gleadow, A., & Fitzgerald, P. G. (1989). The significance of the partial annealing zone in apatite fission-track analysis: Projected track length measurements and uplift chronology of the Transantarctic Mountains. *Chemical Geology: Isotope Geoscience section*, *79*(4), 295–305. https://doi.org/10.1016/0168-9622(89)90035-3

Wolf, R., Farley, K., & Kass, D. (1998). Modeling of the temperature sensitivity of the apatite (U–Th)/He thermochronometer. *Chemical Geology*, *148*(1–2), 105–114. https://doi.org/10.1016/S0009-2541(98)00024-